Am J Cancer Res 2026;16(2):696-720
www.ajcr.us /ISSN:2156-6976/ajcr0171113

Original Article

Histone methyltransferase SETD2 regulates TKT expression and mediates glycolysis to suppress lung adenocarcinoma progression and improve chemosensitivity

Cong Niu[1], Hongqing Li[2], Ji'an Zhou[2], Weijun Chen[2], Hui Zhao[1]

[1]Department of Respiratory and Critical Care Medicine, The Second Affiliated Hospital of Anhui Medical University, Hefei 230601, Anhui, China; [2]Department of Respiratory Medicine, Huadong Hospital, Fudan University, Shanghai 200040, China

Received December 29, 2025; Accepted February 11, 2026; Epub February 25, 2026; Published February 28, 2026

Abstract: Histone methyltransferase SETD2 is frequently downregulated in various malignancies and plays a critical role in regulating tumor progression. However, its biological role in lung adenocarcinoma (LUAD), especially its regulation of glycolysis and chemosensitivity, has not been fully elucidated. Transketolase (TKT) is a crucial enzyme in glycolysis, but whether it is involved in the regulation of LUAD progression and chemosensitivity by SETD2 remains unclear. Cisplatin (CIS)-resistant cells were established, and SETD2 and TKT expression levels were assessed via Western blot. The malignant phenotype of LUAD cells was evaluated through CCK-8 assay, scratch healing, colony formation, and Transwell assay; while apoptosis was determined by flow cytometry. The binding relationship between SETD2 and TKT was verified by ChIP and dual luciferase reporter gene assays. Glycolytic activity was measured using commercial kits. A LUAD tumor model was established in nude mice, and apoptosis and proliferation were detected by TUNEL staining and Ki-67 immunohistochemistry, respectively. SETD2 expression was diminished in LUAD tissues and CIS-resistant cell lines. Overexpression of SETD2 attenuated the malignant phenotype of LUAD cells, promoted apoptosis, and increased the chemosensitivity of CIS-resistant cells. Meanwhile, SETD2 overexpression reduced the glycolytic activity in LUAD cells, as evidenced by decreased glucose uptake, ATP and lactate production, and downregulation of key proteins in the glycolytic pathway. Mechanistically, SETD2 bound to the TKT promoter and suppressed its transcription. Furthermore, TKT overexpression partially reversed the regulatory impacts of SETD2 on LUAD cells. Additionally, SETD2 overexpression suppressed tumor growth by down-regulating TKT, reduced glycolysis level in tumor tissues, promoted apoptosis and inhibited proliferation of tumor cells. In conclusion, SETD2 inhibits glycolysis by directly suppressing TKT transcription, thereby attenuating malignant progression and enhancing chemosensitivity in LUAD.

Keywords: Lung adenocarcinoma, SET domain-containing protein 2, Transketolase, Cis-platinum, glycolysis

Introduction

According to the U.S. Cancer Report, approximately 226,650 new lung cancer cases and 124,730 related deaths were projected for 2025 [1]. China, a high-incidence region for lung cancer, was expected to report over 680,000 new cases in 2024 [2]. As the most prevalent subtype of lung cancer, lung adenocarcinoma (LUAD) accounts for roughly 35-40% of total lung cancer diagnoses [3, 4]. Pathologically, the malignant progression of LUAD is closely associated with epigenetic disorders and metabolic reprogramming [5, 6]. Among them, glycolysis, a central metabolic feature of tumor cells, supplies energy and biosynthetic precursors for tumor proliferation [7]. In recent years, although therapeutic approaches, including surgery, targeted therapies, and immunotherapies, have improved the prognosis of LUAD patients, their 5-year survival rate remains low [8, 9]. In addition, LUAD patients are highly susceptible to drug resistance after chemotherapy, severely compromising treatment efficacy [10, 11]. Therefore, elucidating the molecular mechanisms underlying LUAD

https://doi.org/10.62347/JUWP3285

progression and chemoresistance, and identifying potential therapeutic targets, are of great significance to improve patient prognosis.

Histone methyltransferase SET domain-containing 2 (SETD2) serves as a pivotal regulator in the epigenetic network, catalyzing histone H3 lysine 36 trimethylation (H3K36me3) [12, 13]. H3K36me3, as an important transcriptional activation marker, is involved in multiple biological processes, including gene transcription regulation, chromatin remodeling, and DNA damage repair [14]. Recent investigations have indicated that SETD2 is downregulated in multiple malignant tumors, including renal, colorectal and pancreatic cancers, with its loss or down-regulation strongly correlating with tumor proliferation and poor prognosis [15-17]. Additionally, previous studies have demonstrated that SETD2 deficiency enhances glycolytic flux in pancreatic cancer cells, thereby regulating tumor metabolic reprogramming [18]. Importantly, SETD2 expression is significantly downregulated in LUAD, and SETD2-null tumors exhibit enhanced mitochondrial function, which in turn promotes oxidative metabolism [19]. However, whether SETD2 affects LUAD progression and chemotherapy sensitivity through glycolysis regulation has not been systematically elucidated.

Transketolase (TKT) functions as a core enzyme of the non-oxidative pentose phosphate pathway (PPP). It catalyzes the Transketolase reaction between ketose and aldose to regulate the glycolysis rate and maintain the metabolic balance of tumor cells [20, 21]. TKT exhibits elevated expression in various tumors, including LUAD, and its expression level correlates positively with tumor malignancy, poor survival, and chemotherapy resistance [22-24]. In gliomas, TKT-null cells were more sensitive to the chemotherapeutic agents Temozolomide and cisplatin (CIS), indicating that TKT inhibition may reverse the drug-resistant phenotype [25]. In addition, SETD2 transcriptionally represses TKT, indicating TKT as a critical downstream effector of SETD2-mediated tumor suppression [18].

Given the aforementioned findings, we hypothesized that SETD2 suppresses glycolysis by inhibiting TKT expression, thereby enhancing chemosensitivity in LUAD. This study aims to systematically investigate the regulatory roles of SETD2 in LUAD malignant phenotype, glycolytic metabolism, and chemosensitivity, and to verify whether SETD2 exerts its tumor-suppressive function direct suppression of TKT.

Materials and methods

Cell culture

Human embryonic kidney cells HEK293T (EDC00001) and LUAD cell lines A549 (EDC-00020), PC9 (EDC00363), H1299 (EDC00295), and H460 (EDC00286) were purchased from Guangzhou Editgene Co., Ltd. (Guangdong, China). All cells were cultured in RPMI-1640 medium (R999297, Macklin, Shanghai, China) containing 1% Penicillin-Streptomycin and 10% fetal bovine serum. Incubation was maintained at 37°C in an environment with 5% CO_2 (v/v).

Construction of drug-resistant cell line

H1299 and A549 cells in logarithmic growth phase were seeded in fresh RPMI-1640 medium supplemented with 0.5 μM CIS (HY-17394, MedChemExpress, Monmouth Junction, NJ, USA) and incubated for 48 h. Cell growth was monitored, after which dead cells were removed by rinsing with PBS. Then, complete medium was introduced to continue cultivation. When cells confluence reached approximately 80-90%, the medium was replaced with fresh medium containing 0.5 μM CIS, and this induction process was repeated 3-5 times.

After stable passaging was achieved in medium containing 0.5 μM CIS, the CIS concentration was increased to 1 μM and incubated for 48 h. The above steps were repeated with gradually increasing CIS concentrations until A549 and H1299 cells were able to passage stably under 6 μM CIS. These cells were considered drug-resistant and were designated as H1299/DDP and A549/DDP, respectively [26].

Bioinformatics analysis

GEPIA2 database (http://gepia2.cancer-pku.cn/#index) was employed to analyze the differential expression of SETD2 between LUAD tumor tissues and normal lung tissues. The median SETD2 expression was used as the cutoff value, and patients were assigned into SETD2 high-expression and low-expression groups. The association between SETD2 expression and the prognosis of LUAD patients was subsequently analyzed.

Cell transfection and treatment

SETD2 overexpression plasmid (OE-SETD2), TKT overexpression plasmid (OE-TKT), SETD2 catalytic mutant plasmid (OE-SETD2$^{\Delta CAT}$), SETD2 small interfering RNA (si-SETD2), TKT small interfering RNA (si-TKT), and their corresponding controls (OE-NC, si-NC) were constructed by Sangon Biotech Co., Ltd. (Shanghai, China).

Plasmids were transfected into H1299 and A549 cells, as well as H1299/DDP and A549/DDP cells for 48 h using Lipofectamine 3000 (L3000001, Invitrogen, Carlsbad, CA, USA) according to the manufacturer's instructions. Transfection efficiency was assessed by detecting SETD2 and TKT protein expression in cells.

In addition, when exploring the effect of SETD2 on cellular chemosensitivity, different plasmids were first transfected into H1299/DDP and A549/DDP cells, which were then treated with CIS for 48 h.

Cell Counting Kit-8 (CCK-8) assay

H1299 and A549 cells were inoculated into 96-well plates at a density of approximately 1×10^4 cells/well and incubated overnight to allow cell attachment. Then, cells were treated with different concentrations of CIS (6.25, 12.5, 25, 50 μM) for 48 h. 10% CCK-8 reagent (C917226, Macklin) was subsequently added, mixed thoroughly, and incubated for 2 h in a light-protected environment. Absorbance at OD_{450} values was determined using a microplate reader (1410101, Thermo Fisher Scientific, Waltham, MA, USA).

Scratch-wound assay

LUAD cells were inoculated in 6-well plates (2×10^5 cells/mL) and cultured until cell confluence reached 90%. A 20 μL pipette tip was utilized to scratch a straight line across the center of the cell monolayer in each well. Cell debris generated during the scratching process was washed with PBS, followed by the addition of serum-free medium. After 24 h, images were captured, and the migration distance was quantified using ImageJ software (1.54h version, National Institute of Mental Health, MD, USA).

Clone formation assay

H1299 and A549 cells were gently rinsed with PBS and resuspended to obtain single-cell suspensions. Cells were seeded into 6-well plate at a density of 1×10^4 cells per well in 1 mL of culture medium, and the culture medium was subsequently refreshed every 2-3 d for 14 d. When clear cell clusters were observed by the naked eye, the culture was terminated, and cells were fixed with 4% paraformaldehyde (P885233, Macklin) for 30 min. Subsequently, colonies were stained with 1% crystal violet (C916088, Macklin) for 10 min, and excess stain was gently rinsed away with PBS. The culture plates were allowed to dry naturally, and the cell clones were observed using a CX33 light microscope (Olympus, Tokyo, Japan).

Transwell assay

Matrigel (354230, Corning, Tewksbury, MA, USA) was thawed at room temperature and diluted 1:8 with serum-free culture solution. The diluted Matrigel (100 μL) was pipetted and evenly covered on the bottom of the Transwell chamber (8 μm, Corning). Each well of the 24-well plate was supplemented with 600 μL of culture medium, after which the inserts were slowly placed into the wells.

A549 and H1299 cell suspensions (4×10^5/mL, 100 μL per well) were inoculated into the upper chamber and incubated at 37°C for 48 h. After incubation, the inserts were rinsed with PBS and then fixed with 4% paraformaldehyde for 15 min. Non-invading cells in the upper chamber were wiped away using a sterilized cotton swab. Cells on the lower surface of the chambers were stained with 0.1% crystal violet (HY-B0324A, MedChemExpress) for 20 min and rinsed with running water. Light microscopy was employed to acquire images of five randomly chosen fields of view, followed by the counting of invaded cell numbers with the assistance of ImageJ 1.54h software [27].

Apoptosis assay

After the indicated treatments, H1299 and A549 cells were harvested and resuspended in 500 μL Annexin V Binding Buffer (A709121, Macklin). Next, 5 μL of Annexin-V-FITC and 5 μL of propidium iodide (PI) were introduced sequentially, mixed thoroughly, and incubated

for 15 min in a light-protected environment. Detection was conducted with a flow cytometer (BD FACSCalibur™, BD biosciences, CA, USA), and the resulting data were analyzed with FlowJo software (v10.8, BD biosciences) to calculate apoptosis rates.

Determination of glucose uptake and lactate production

After cell transfection, H1299 and A549 cells were rinsed with PBS and homogenized under ice-cold conditions. Cell lysates and Glucose Uptake Detection Buffer were added into 96-well plates according to kit's instructions (S0554S, Beyotime, Shanghai, China). Following incubation at 37°C for 30 min under light-protected conditions, and the OD450 value was measured to determine cellular glucose uptake. In addition, lactate levels in cell culture supernatants were quantified using a lactate assay kit (S0208S, Beyotime) [28].

Extracellular acidification rate (ECAR) determination

H1299 and A549 cells were seeded in Seahorse XF96 cell culture plates (4×10^4/well). Cellular ECAR levels were then measured using the Seahorse XF Pro Analyzer (Agilent Technologies, CA, USA) according to the instructions of the Seahorse XF Glycolytic Stress Test Kit (103020-100, Agilent Technologies) [29].

Chromatin immunoprecipitation (ChIP)-qPCR

ChIP assay was performed using the SimpleChIP® Plus sonolysis ChIP kit (56383, Cell Signaling Technology, MA, USA) [30]. H1299 and A549 cells were cross-linked with 1% formaldehyde solution at 37°C for 10 min, and cross-linking was terminated with glycine. Cells were rinsed with PBS, collected, lysed on ice, and subjected to sonication for fragmentation. The resulting chromatin was then incubated overnight at 4°C with anti-SETD2 (PA5-34934, Invitrogen) or IgG antibody (2729, Cell Signaling Technology). After DNA recovery, qPCR was performed using primers targeting the TKT promoter region (F: 5'-GGTCTCAAGAAGGCCACTCC-3', R: 5'-GCTGGGGTGTGTGTGTTAAC-3').

Dual-Luciferase reporter assay

Wild-type (WT) and mutant-type (MUT) dual-luciferase reporter plasmids targeting the TKT promoter region were synthesized by Sangon Biotech Co., Ltd. Combinations of TKT-WT with OE-NC or OE-SETD2, TKT-WT with si-NC or si-SETD2, TKT-MUT with OE-NC or OE-SETD2, TKT-MUT with si-NC or si-SETD2 were co-transfected into A549 cells using Lipofectamine 3000, respectively. After 48 h of incubation, cells were harvested, and luciferase activity was measured using the Dual-Lucy Assay Kit (RG027, Beyotime) [31].

Subcutaneous xenograft model in nude mice

Five-week-old BALB/c nude mice (15-18 g) were obtained from Vital River (Beijing, China) and housed at 22°C, with 45% relative humidity and a 12-hour light-dark cycle. After one week of acclimatization, mice were used to construct a subcutaneous xenograft tumor model. OE-NC, OE-SETD2, OE-SETD2+OE-NC, and OE-SETD2+OE-TKT were transfected in A549 cells. Each mouse was subcutaneously injected with 100 μL of the corresponding cell suspension at the right axilla region. The animals were then divided into four groups according to the transfected cells, designated as the OE-NC, OE-SETD2, OE-SETD2+OE-NC, and OE-SETD2+OE-TKT groups, respectively. Tumor growth was observed weekly, and tumor length and width were measured using vernier calipers. On the 28th day post-inoculation, mice were euthanized via intraperitoneal injection of pentobarbitalic acid (100 mg/kg). Subsequently, the tumors were completely excised with tissue scissors, and their mass was weighed and photographically documented.

Additionally, OE-NC, OE-SETD2, OE-SETD2+OE-NC, and OE-SETD2+OE-TKT were transfected in A549/DDP cells, respectively. 100 μL of successfully transfected A549/DDP cell suspension was injected subcutaneously into the right axilla of nude mice, and when the tumor volume reached 100 mm^3, CIS (4 mg/kg) was injected intraperitoneally twice a week [32]. Tumor growth was observed weekly, and tumor size was measured. On day 28, mice were euthanized by intraperitoneal injection of Pentobarbital Sodium (100 mg/kg), and tumors were euthanized, weighed, and photographed. All animal experimental protocols in this study were reviewed and approved by the Huadong Hospital, Fudan University Ethics Committee (NO.2023-HDYY-40JZS). All animal experiments are conducted in strict compliance with the Guide for

the Care and Use of Laboratory Animals and the ARRIVE Guide 2.0.

TUNEL staining

After being fixed in 4% paraformaldehyde solution for 24 hours, tumor tissues were dehydrated with gradient ethanol series and paraffin embedded. Paraffin sections were prepared as 4 μm-thick serial sections. Subsequently, sections were deparaffinized with xylene (X821391, Macklin) and then rehydrated via gradient ethanol solution. Tissue sections were then incubated with DNase-free proteinase K (20 μg/mL, HY-108717A, MedChemExpress) at 37°C for 15 min, followed by incubation with TUNEL assay solution (C1086, Beyotime) for 60 min in the dark. The tissues were then counterstained with DAPI staining solution (C1006, Beyotime), for 10 min in the dark and photographed using a BX53 fluorescence microscope (Olympus).

Immunohistochemistry

Paraffin-embedded tumor tissue sections were deparaffinized and rehydrated through gradient ethanol. Antigen retrieval was performed by microwave heating citrate buffer (pH=6.0). Endogenous peroxidase activity was blocked by incubation with 3% H_2O_2 solution for 30 min, followed by washing with PBS. Tissue sections were blocked with 5% bovine serum albumin (BSA, GA527, Beyotime) for 30 min and then incubated with primary antibody against Ki-67 (ab92742, 1:500, Abcam, MA, USA) at 37°C for 90 min. After washing, sections were incubated with goat anti-rabbit IgG secondary antibody (31466, 1:500, Invitrogen) for 30 min. After that, color development was performed using DAB substrate (P0203, Beyotime) for 20 min and then terminated by rinsing with distilled water. Cell nuclei were counterstained with hematoxylin staining solution (HY-N0116, MedChemExpress), and then observed under a light microscope.

Adenosine triphosphate (ATP) levels and lactate dehydrogenase (LDH) activity measurements

ATP content in nude mouse tumor tissues and LUAD cells was determined by an ATP assay kit (S0026, Beyotime). 20 mg of tumor tissue was homogenized in 200 μL of lysate buffer, and the supernatant was collected after centrifugation. The ATP level in the tissue was determined according to the manufacturer's instructions.

For A549 and H1299 cells, culture medium was aspirated, cells were lysed in 200 μL of lysate buffer, and the supernatant was collected by centrifugation to determine ATP levels. In addition, LDH activity in the supernatant of tumor tissue homogenates was detected using an LDH activity assay kit (AK141, BIOSS, Beijing, China).

Western blot (WB)

Tumor tissues were minced into pieces, lysed in cell lysis buffer (C718615, Macklin), and ground thoroughly in an ice bath. H1299 and A549 cells were first rinsed with PBS and subsequently lysed using lysis buffer. After centrifugation, the protein content in the supernatant was determined using a BCA kit (B917925, Macklin). Equal amounts of proteins were separated using SDS-PAGE electrophoresis and transferred to PVDF membranes (Invitrogen). Then, the membranes were blocked with 5% BSA at 25°C for 2 h. After washing, the membrane was incubated overnight at 4°C with indicated primary antibody. After washing with TBST, the membrane was incubated with sheep anti-rabbit secondary IgG (1:10,000) for 2 h at 25°C. The ECL luminescent solution (E917968, Macklin) was evenly dripped onto the membrane and visualized using a JP-2880 gel imaging system (Jinpeng Analysis Instrument Co., Ltd., Shanghai, China). ImageJ software was employed to determine the gray value of protein bands, with GAPDH (MA5-35235, 1:50,000, Invitrogen) serving as the loading control; based on these values, the relative protein expression was computed.

The primary antibodies included glucose transporter 1 (GLUT1, ab115730, 1:10000, Abcam), SETD2 (ab239350, 1:1000, Abcam), H3K36me3 (PA5-17109, 1:2000, Invitrogen), Lactate Dehydrogenase A (LDHA, ab300638, 1:1000, Abcam), hexokinase 1 (HK1, ab150423, 1:2000, Abcam), hexokinase 2 (HK2, ab227198, 1:5000, Abcam), TKT (ab112997, 1:1000, Abcam), multidrug resistance-associated protein 1 (MRP1, ab260038, 1:1000, Abcam), ATP-binding cassette sub-family B member 1 (ABCB1, MA5-32282, 1:2000, Invitrogen), ATP binding cassette subfamily G member 2 (ABCG2, ab207732, 1:1000, Abcam), Histone

H3 (H3, ab1791, 1:2000, Abcam), and phosphoglycerate kinase 1 (PGK1, ab199438, 1:1000, Abcam).

Statistical analysis

Each experiment was repeated in triplicates, with the data expressed as mean ± standard deviation. Statistical analyses were performed using IBM SPSS Statistics software (version 26.0). For comparisons between two groups, Student's t-test was applied when data followed normality and homogeneity of variance, whereas the Satterthwaite-corrected t-test was used when variances were unequal. If data did not follow a normal distribution, the nonparametric Wilcoxon rank sum test was used. One-way analysis of variance (ANOVA) was performed to evaluate differences among multiple groups, followed by LSD test for post-hoc pairwise comparison. For data involving multiple time points, repeated measures analysis of variance was used to evaluate the main effects of group, time, and the group-time interaction, with Bonferroni-corrected pairwise t-tests for subsequent comparisons. A p value<0.05 was considered statistically significant. All figures were plotted using Prism software (Graphpad 9.0).

Results

SETD2 overexpression inhibited the malignant phenotype and induced apoptosis of LUAD cells

Analysis of the GEPIA2 database revealed that SETD2 was notably downregulated in LUAD tissues compared with normal lung tissues. Although no significant difference was observed in overall survival between SETD2 high and low expression groups, patients in the high-expression exhibited a trend toward improved overall survival, suggesting its potential prognostic value (**Figure 1A**, **1B**). WB analysis indicated that SETD2 and its downstream product H3K36me3 were highly expressed in HEK293T cells but markedly reduced in LUAD cell lines. Among these, H1299 and A549 cells displayed the most pronounced reduction in SETD2 and H3K36me3 expression (**Figure 1C-E**).

To explore the regulatory impact of SETD2 on the malignant phenotype of LUAD, OE-SETD2 and si-SETD2 were transfected into H1299 and A549 cells, respectively. Transfection of OE-SETD2 markedly raised SETD2 and H3K36me3 levels in both cells, while transfection of si-SETD2 effectively reduced the expression, confirming successful transfection (**Figure 1F-H**).

CCK-8 assay demonstrated that transfection of OE-SETD2 remarkably reduced the viability of H1299 and A549 cells, while transfection of si-SETD2 notably enhanced cell viability (**Figure 1I**, **1J**). In addition, SETD2 overexpression significantly reduced the number of colonies formed and wound healing rate in LUAD cells, whereas SETD2 knockdown exerted the opposite effects (**Figure 1K-P**). As revealed by Transwell assay, invasive cells in the SETD2 overexpression group were notably reduced, but markedly increased in the SETD2 knockdown group (**Figure 1Q-S**).

Furthermore, transfection with OE-SETD2 significantly elevated the apoptosis rate, while transfection with si-SETD2 exerted the opposite effect (**Figure 1T-V**).

Collectively, these results confirmed that SETD2 is downregulated in LUAD and that its overexpression effectively suppresses malignant phenotypes and promotes apoptosis in LUAD cells.

SETD2 overexpression increased chemosensitivity of LUAD cells

Next, CIS-resistant H1299/DDP and A549/DDP cells were established to investigate the role of SETD2 in regulating chemosensitivity of resistant cells. Following treatment with increasing concentrations of CIS, the IC50 values of H1299, H1299/DDP, A549, and A549/DDP cells were 14.85, 45.9, 13.92, and 49.18 μM, respectively, with a resistance index of approximately 3, confirming the successful construction of drug-resistant cells (**Figure 2A**, **2B**).

Consistently, the expression levels of drug resistance-related proteins, including MRP1, ABCB1, and ABCG2, were significantly upregulated in H1299/DDP and A549/DDP cells compared with their corresponding parental cells (**Figure 2C-E**). Compared with their parental H1299 and A549 cells, SETD2 and H3K36me3 levels were markedly decreased in both H1299/DDP and A549/DDP cells (**Figure 2F-H**), imply-

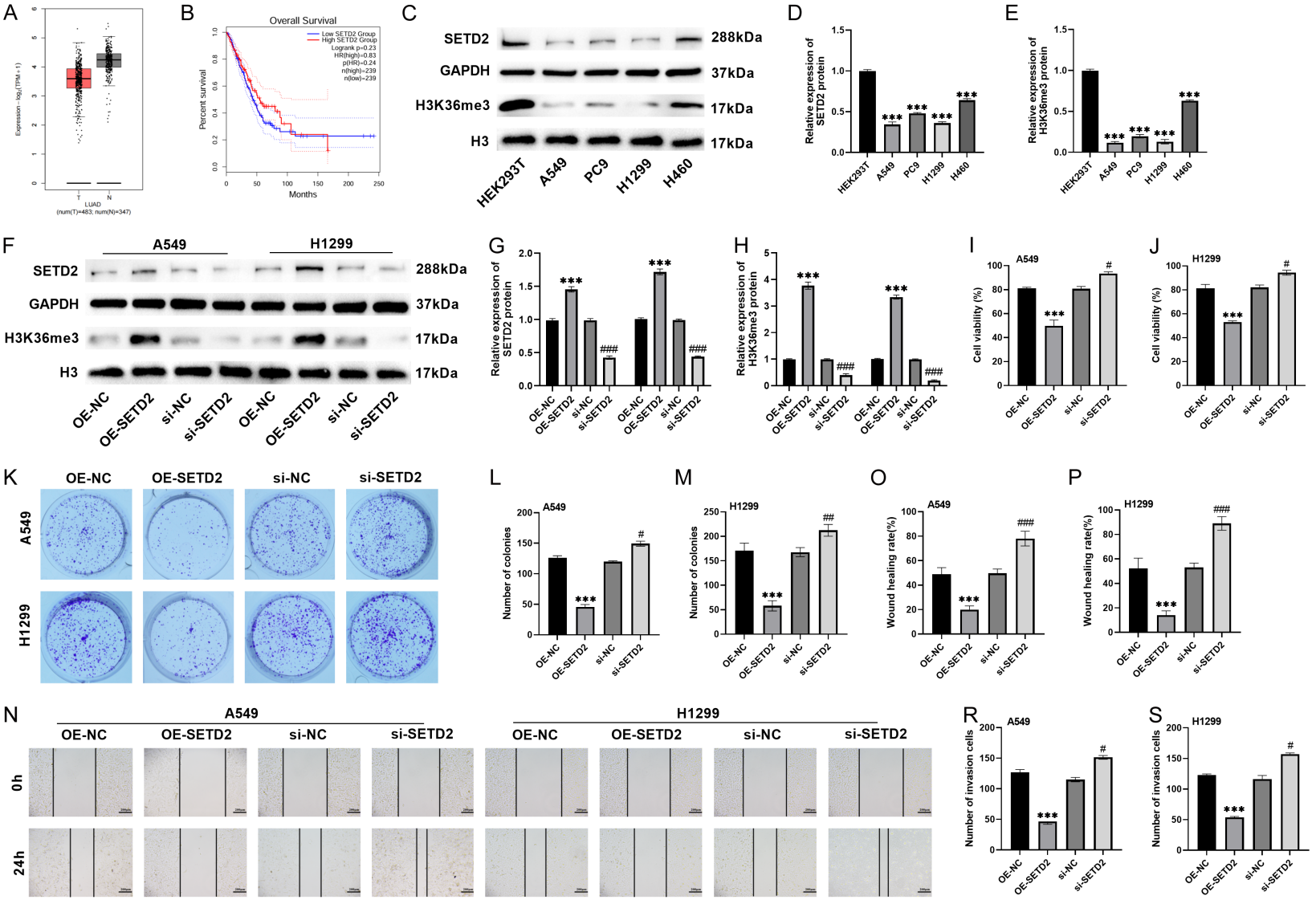
A
B
Overall Survival
Low SETD2 Group
High SETD2 Group
Months
C
SETD2
GAPDH
H3K36me3
H3
288kDa
37kDa
17kDa
17kDa
HEK293T
A549
PC9
H1299
H460
D
Relative expression of SETD2 protein
E
Relative expression of H3K36me3 protein
F
A549
H1299
OE-NC
OE-SETD2
si-NC
si-SETD2
G
Relative expression of SETD2 protein
H
Relative expression of H3K36me3 protein
I
Cell viability (%)
J
K
L
Number of colonies
M
O
Wound healing rate(%)
P
N
0h
24h
R
Number of invasion cells
S

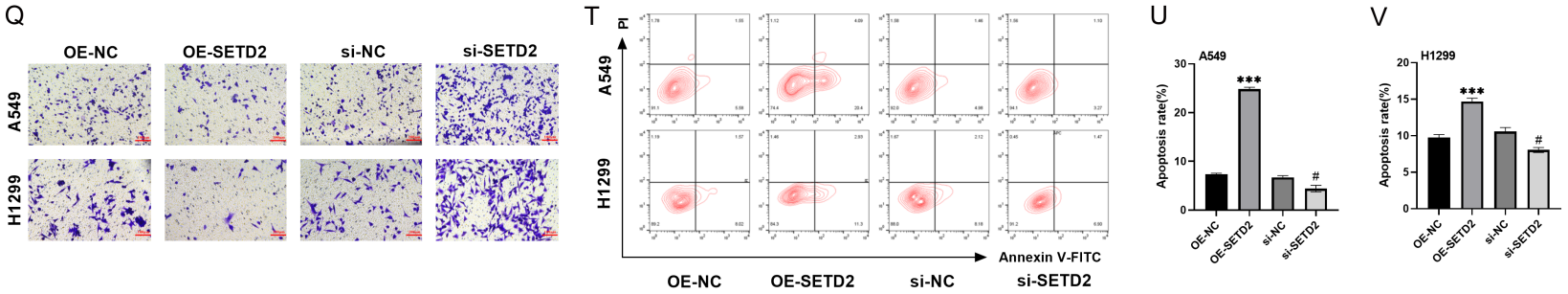

Figure 1. SETD2 overexpression inhibited malignant phenotypes and induced apoptosis in LUAD cells. A. Expression of SETD2 in LUAD and normal lung tissues. B. Overall survival of LUAD patients with high and low SETD2 expression. C-E. WB analysis of SETD2 and H3K36me3 expression in HEK293T cells and LUAD cells. F-H. Transfection of OE-SETD2 increased SETD2 and H3K36me3 protein levels in H1299 and A549 cells, whereas si-SETD2 transfection decreased SETD2 and H3K36me3 protein levels. I, J. Cell viability assessed by CCK-8 assay after transfection with OE-SETD2 or si-SETD2. K-M. Colony formation assay showing clonogenic capacity after transfection with OE-SETD2 or si-SETD2. N-P. Scratch-wound assay evaluating cell migration after transfection with OE-SETD2 or si-SETD2 (10×, 200 μm). Q-S. Transwell invasion assay assessing invasion capacity after transfection with OE-SETD2 or si-SETD2 (20×, 100 μm). T-V. Apoptosis rate determined by flow cytometry after transfection with OE-SETD2 or si-SETD2. ***P<0.001 vs OE-NC; $^{\#}P$<0.05, $^{\#\#}P$<0.01, $^{\#\#\#}P$<0.001 vs si-NC.

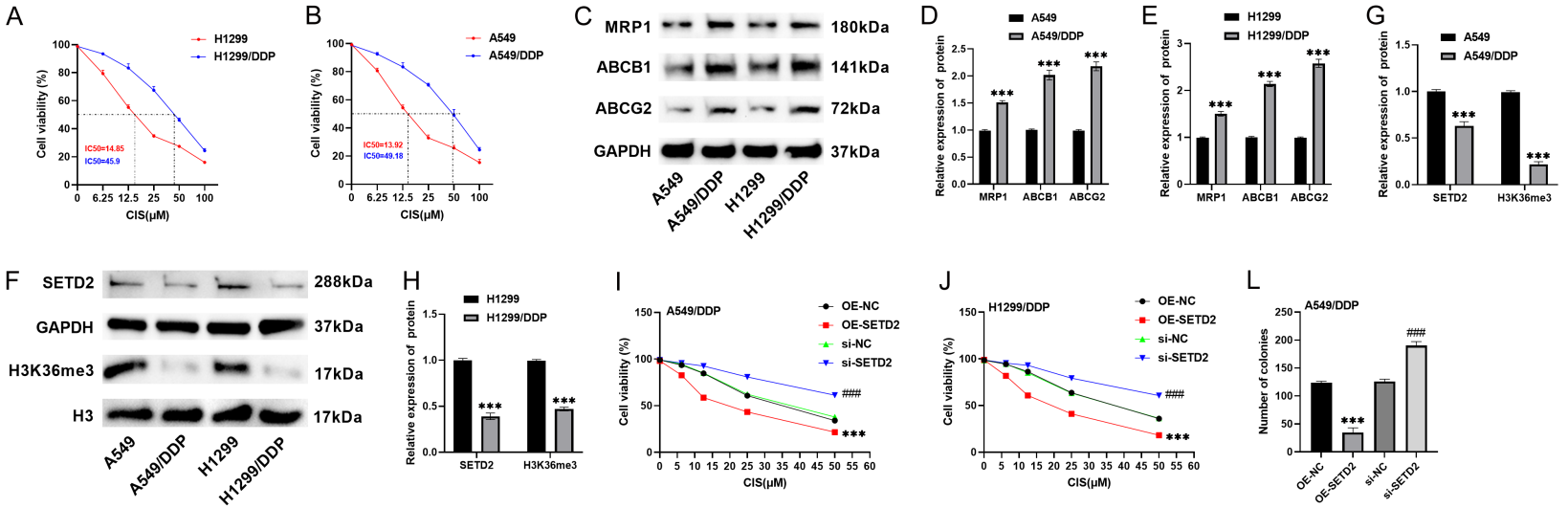

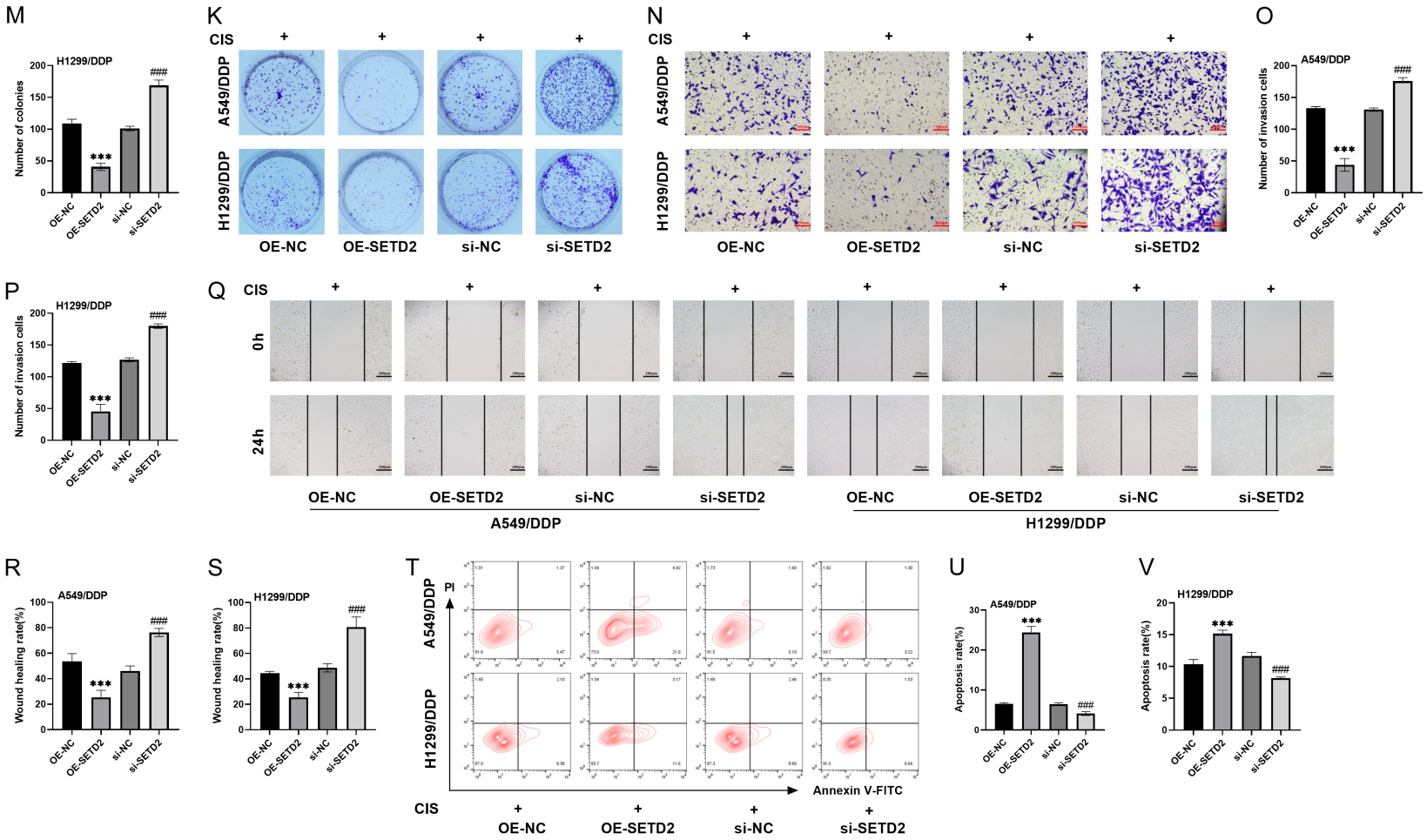

Figure 2. SETD2 overexpression enhanced chemosensitivity of LUAD cells. A, B. Cell viability assessed by CCK-8 assay, and the IC50 value of CIS in H1299, H1299/DDP, A549, and A549/DDP cells. C-E. WB analysis of drug resistance-related proteins (MRP1, ABCB1, ABCG2) in H1299, H1299/DDP, A549, and A549/DDP cells. F-H. Protein expression levels of SETD2 and H3K36me3 in H1299/DDP and A549/DDP cells assessed by Western blot. I, J. Effects of OE-SETD2 or si-SETD2 transfection on the viability of H1299/DDP and A549/DDP cells after CIS treatment assessed by CCK-8 assay. K-M. Colony formation assay showing clonogenic ability after 12.5 μM CIS treatment. N-P. Transwell invasion assay assessing the number of invaded cells after CIS treatment (20×, 100 μm). Q-S. Scratch-wound assay evaluating cell migration after CIS treatment (10×, 200 μm). T-V. Apoptosis rate of H1299/DDP and A549/DDP cells assessed by flow cytometry. ***P<0.001 vs OE-NC; ###P<0.001 vs si-NC.

ing a close association between SETD2 downregulation and CIS resistance in LUAD cells.

To further verify the functional role of SETD2 in drug resistance, OE-SETD2 and si-SETD2 were transfected into H1299/DDP and A549/DDP cells followed by treatment with different concentrations of CIS. Transfection of OE-SETD2 markedly reduced the cell viability of drug-resistant cells under CIS exposure, whereas transfection of si-SETD2 enhanced cell viability (**Figure 2I**, **2J**). The impact of SETD2 overexpression was most pronounced at a CIS concentration of 12.5 μM, which was selected for subsequent experiments.

Overexpression of SETD2 notably decreased colony formation, invasion ability, and scratch healing rates in CIS-treated drug-resistant cells, while SETD2 knockdown significantly promoted these malignant phenotypes (**Figure 2K-S**). Additionally, transfection of OE-SETD2 markedly increased apoptosis in CIS-treated drug-resistant cells, whereas transfection of si-SETD2 exerted the opposite effects (**Figure 2T-V**). These findings suggest that SETD2 is downregulated in CIS-resistant LUAD cells and that its overexpression effectively restores chemosensitivity of CIS-resistant cells.

SETD2 overexpression suppressed glycolysis in LUAD cells

To elucidate the mechanism underlying the suppressive effect of SETD2 on the malignant phenotype of LUAD cells, its role in regulating glycolysis was explored. Overexpression of SETD2 in H1299 and A549 cells significantly reduced glucose uptake (**Figure 3A**, **3B**), lactate production, the major end product of glycolysis (**Figure 3C**, **3D**), and ATP content (**Figure 3E**, **3F**). However, SETD2 knockdown markedly raised glucose uptake, ATP content, and lactate production, suggesting that SETD2 may exert an inhibitory effect on glycolysis metabolism in LUAD cells.

In addition, SETD2 overexpression significantly decreased the extracellular acidification rate (ECAR), while SETD2 knockdown significantly increased ECAR (**Figure 3G**, **3H**), indicating that SETD2 suppresses glycolytic activity of LUAD cells. Moreover, SETD2 overexpression significantly down-regulated GLUT1, HK1, HK2, PGK1 and LDHA protein expression. On the contrary, SETD2 knockdown reversed the expression patterns of these proteins (**Figure 3I-N**). These findings imply that SETD2 inhibits glycolysis by downregulating glycolysis-related proteins in LUAD cells.

SETD2 negatively regulated TKT expression

Next, the downstream target genes of SETD2 in regulating glycolysis in LUAD cells were investigated to provide insight into the molecular mechanism by which SETD2 functions as a tumor suppressor. Western blot analysis showed that TKT protein level was significantly increased in H1299 and A549 cells compared with HEK293T cells. This expression pattern was inversely correlated with that of SETD2 in these cell lines (**Figure 4A**, **4B**). To verify the regulatory relationship between SETD2 and TKT, OE-SETD2 and si-SETD2 were transfected into H1299 and A549 cells, respectively. Overexpression of SETD2 notably reduced TKT protein levels, while SETD2 knockdown increased TKT protein level (**Figure 4C**, **4D**), indicating that SETD2 exerted a negative regulatory effect on TKT.

ChIP combined with qPCR assay showed that TKT was significantly enriched in the SETD2 gene body region (**Figure 4E**, **4F**). In addition, dual-luciferase reporter assays were performed using reporter constructs containing the wild-type (TKT-WT) or mutant (TKT-MUT) TKT promoter regions. Overexpression of SETD2 notably suppressed the luciferase activity in TKT-WT group, whereas SETD2 knockdown enhanced it; however, no marked effect was observed in TKT-MUT group, confirming that SETD2 directly regulates TKT transcription (**Figure 4G**, **4H**).

To further determine whether this transcriptional repression depends on SETD2 catalytic activity, an OE-SETD2$^{\Delta CAT}$ construct was generated, which retains chromatin-binding ability but lacks H3K36me3 methyltransferase activity. Compared with the OE-NC group, the OE-SETD2 group showed significantly decreased TKT protein expression and significantly increased H3K36me3 levels; however, in the OE-SETD2$^{\Delta CAT}$ group, TKT protein expression and H3K36me3 levels were not significantly different from those in the OE-NC group, but differed significantly from the OE-SETD2 gro-

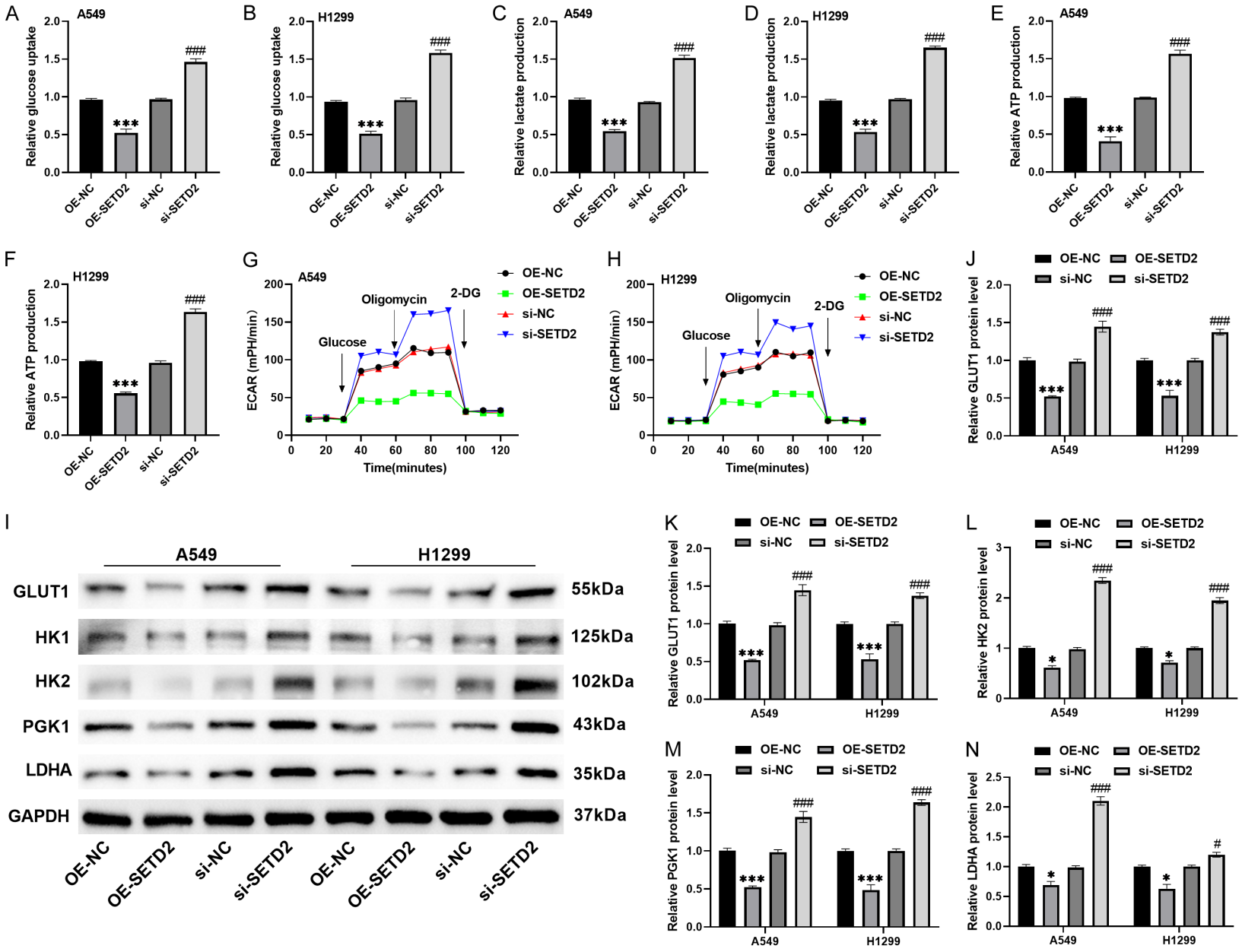
A
A549
Relative glucose uptake
B
H1299
Relative glucose uptake
C
A549
Relative lactate production
D
H1299
Relative lactate production
E
A549
Relative ATP production
F
H1299
Relative ATP production
OE-NC
OE-SETD2
si-NC
si-SETD2
G
A549
ECAR (mPH/min)
Glucose
Oligomycin
2-DG
Time(minutes)
H
H1299
ECAR (mPH/min)
Glucose
Oligomycin
2-DG
Time(minutes)
J
Relative GLUT1 protein level
A549
H1299
I
A549
H1299
GLUT1
HK1
HK2
PGK1
LDHA
GAPDH
55kDa
125kDa
102kDa
43kDa
35kDa
37kDa
K
Relative GLUT1 protein level
L
Relative HK2 protein level
M
Relative PGK1 protein level
N
Relative LDHA protein level

Figure 3. SETD2 overexpression reduced glycolysis in LUAD cells. (A-F) SETD2 overexpression decreased glucose uptake (A, B), lactate production (C, D), and ATP content (E, F) in A549 and H1299 cells, while knockdown of SETD2 exerted opposite effects. (G, H) SETD2 overexpression decreased ECAR, while knockdown of SETD2 increased ECAR. (I-N) WB analysis of glycolysis-related proteins GLUT1, HK1, HK2, PGK1 and LDHA after SETD2 overexpression or knockdown. Note: ECAR, Extracellular acidification rate. **P*<0.05, ****P*<0.001 vs OE-NC; #*P*<0.05, ###*P*<0.001 vs si-NC.

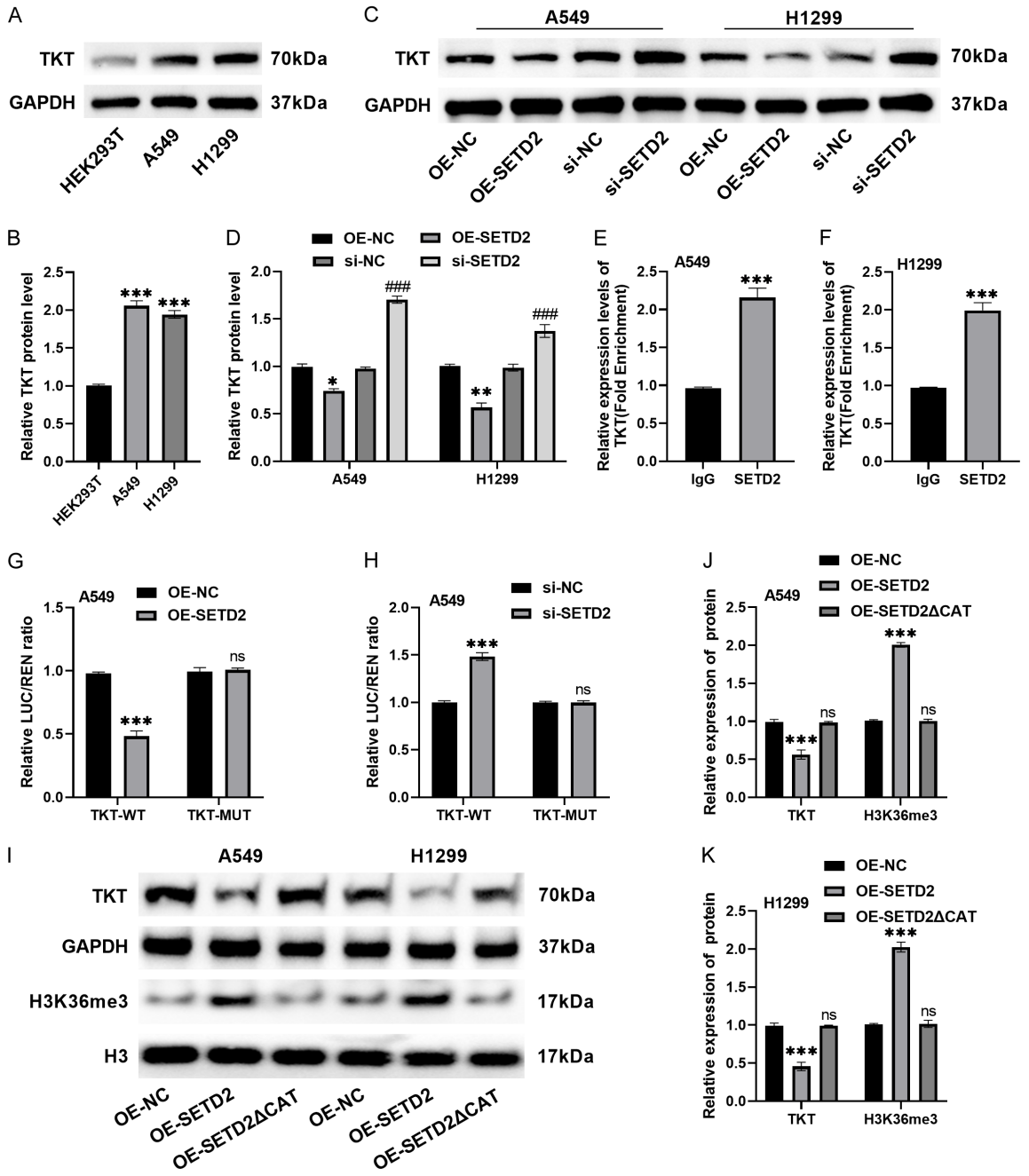

Figure 4. SETD2 negatively regulated TKT expression. A, B. WB analysis of TKT levels in HEK293T cells, A549 and H1299 cells. C, D. Transfection of OE-SETD2 decreased TKT protein levels, whereas transfection of si-SETD2 increased TKT protein levels in A549 and H1299 cells. E, F. ChIP-qPCR analysis showing enriched TKT in SETD2 gene bodies. G, H. Dual-luciferase reporter gene assay demonstrating that TKT is a target of SETD2. I-K. WB analysis of H3K36me3 and TKT protein levels after transfection with OE-SETD2$^{\Delta CAT}$. ns *P*≥0.05, ****P*<0.001 vs OE-NC; ###*P*<0.001 vs si-NC.

up (**Figure 4I-K**). These results suggest that SETD2-mediated transcriptional repression of TKT is dependent on H3K36me3 catalytic activity. Collectively, these results demonstrate that SETD2 negatively regulates TKT expression, and that TKT is a direct downstream target gene of SETD2 in LUAD cells.

SETD2 overexpression inhibited TKT expression and inhibited glycolysis

To test whether TKT mediates the regulation of SETD2 on glycolysis in LUAD cells, OE-TKT and si-TKT were transfected into H1299 and A549 cells. Transfection of OE-TKT markedly increased TKT expression level, while transfection of si-TKT effectively decreased TKT expression level, indicating successful construction of TKT overexpression and knockdown cell models (**Figure 5A**, **5B**). In SETD2-overexpressing cells, overexpression of TKT significantly increased glucose uptake (**Figure 5C**), lactate production (**Figure 5E**), and ATP content (**Figure 5G**); However, knockdown of TKT in SETD2-silenced cells notably reduced glucose uptake (**Figure 5D**), lactate production (**Figure 5F**), and ATP content (**Figure 5H**). Furthermore, TKT overexpression significantly increased ECAR levels, whereas knockdown of TKT led to a pronounced decrease in ECAR levels (**Figure 5I-L**). Moreover, TKT overexpression significantly upregulated the expression of key glycolysis-related proteins, including GLUT1, HK1, HK2, PGK1 and LDHA; conversely, knockdown of TKT downregulated the expression of these proteins, exhibiting a regulatory pattern opposite to that observed with SETD2 overexpression (**Figure 5M-X**). These findings collectively suggest that TKT is a key mediator of SETD2-dependet regulation of glycolysis in LUAD cells.

SETD2 overexpression inhibited the malignant progression and enhanced chemosensitivity of LUAD cells through regulating TKT

Next, whether SETD2 mediates LUAD malignant progression and chemosensitivity through regulation of TKT was investigated. In parental H1299 and A549 cells, the inhibitory effects of SETD2 overexpression on colony formation (**Figure 6A**, **6B**), scratch healing (**Figure 6C**, **6D**), and cell invasion (**Figure 6E**, **6F**) were markedly weakened after co-transfection of OE-SETD2 and OE-TKT. Additionally, co-transfection of OE-TKT significantly reduced the apoptosis rate induced by SETD2 overexpression (**Figure 6G**, **6H**).

In drug-resistant H1299/DDP and A549/DDP cells, co-transfection with OE-TKT significantly enhanced cell viability after CIS treatment, suggesting that TKT overexpression reversed the chemosensitivity-enhancing effect of SETD2 on these drug-resistant cells (**Figure 6I**, **6J**). Similarly, the inhibitory effects of SETD2 overexpression on colony formation (**Figure 6K**, **6L**), scratch healing (**Figure 6M**, **6N**), and cell invasion (**Figure 6O**, **6P**) were significantly attenuated after co-transfection with OE-TKT, accompanied by a significant reduction in apoptosis (**Figure 6Q**, **6R**).

The above results collectively indicated that TKT overexpression effectively reversed the suppressive impact of SETD2 on malignant phenotypes in both parental and drug-resistant cells, confirming that TKT is a key target through which SETD2 inhibits the malignant progression of LUAD and enhances chemosensitivity.

SETD2 overexpression inhibited tumor growth in vivo by regulating TKT

A LUAD tumor model was established in nude mice via subcutaneous injection of A549 cells to investigate whether SETD2 suppresses tumor growth *in vivo*. In the OE-SETD2 group, SETD2 and H3K36me3 expression levels were markedly upregulated, whereas TKT expression was notably reduced. However, co-transfection with OE-TKT decreased SETD2 and H3K36me3 expression levels and significantly increased TKT level *in vivo* (**Figure 7A-D**). Overexpression of SETD2 led to a notable reduction in tumor volume and weight. In contrast, tumors in the OE-SETD2+OE-TKT group exhibited significantly increased volumes and weight, suggesting that overexpression of TKT can attenuate the inhibitory effects of SETD2 on tumor growth (**Figure 7E-G**). TUNEL staining revealed a marked increase in TUNEL-positive cells in the OE-SETD2 group, whereas co-transfection with OE-TKT reduced the proportion of TUNEL-positive cells (**Figure 7H**, **7I**). Immunohistochemistry demonstrated that Ki-67 level was significantly decreased in tumor tissues of OE-SETD2 group, while Ki-67 expression was partially restored after OE-TKT co-transfection (**Figure 7J**, **7K**).

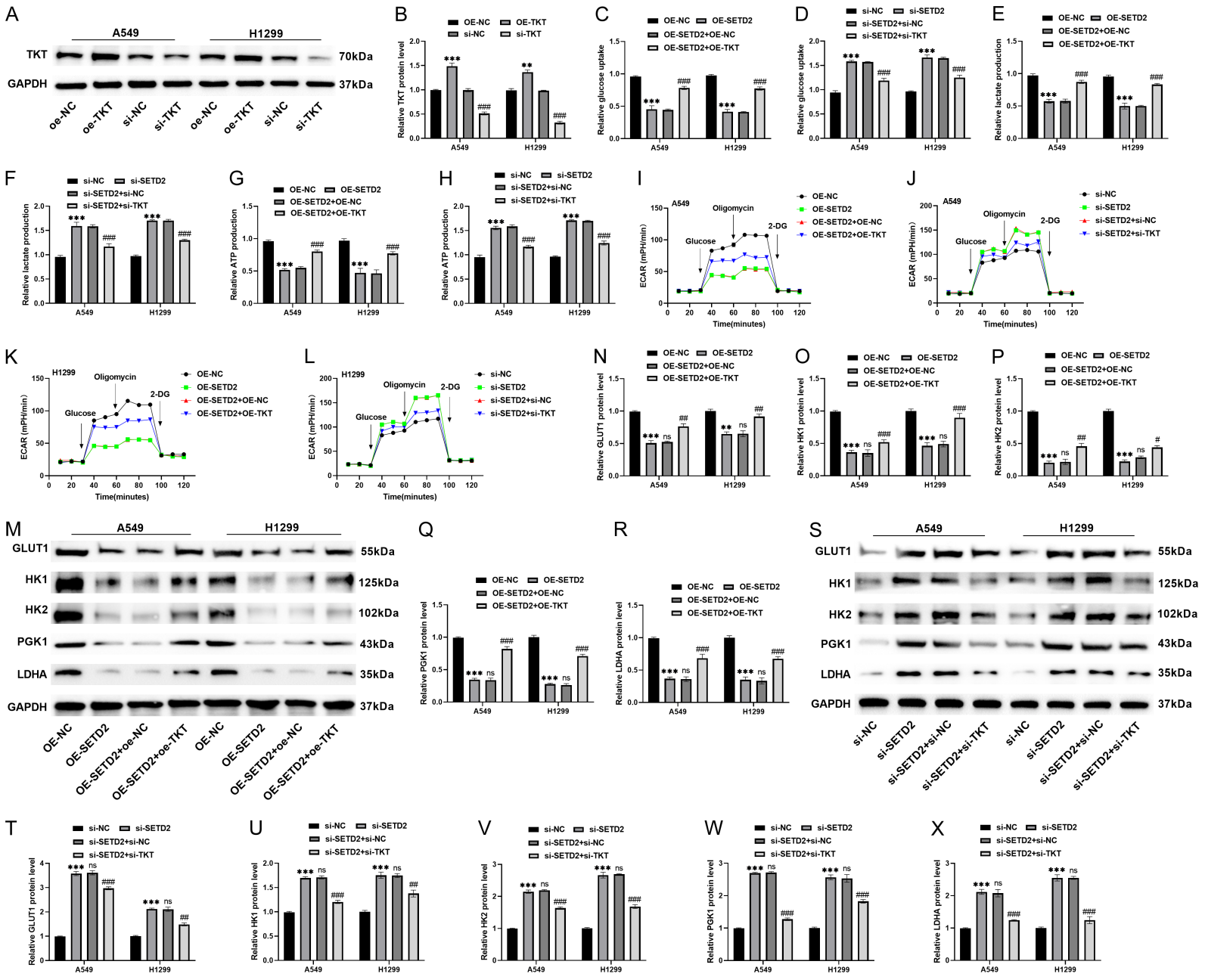
A
A549
H1299
TKT
GAPDH
70kDa
37kDa
oe-NC
oe-TKT
si-NC
si-TKT
B
Relative TKT protein level
C
Relative glucose uptake
D
Relative glucose uptake
E
Relative lactate production
F
Relative lactate production
G
Relative ATP production
H
Relative ATP production
I
ECAR (mPH/min)
Glucose
Oligomycin
2-DG
Time(minutes)
J
K
L
N
Relative GLUT1 protein level
O
Relative HK1 protein level
P
Relative HK2 protein level
M
GLUT1
HK1
HK2
PGK1
LDHA
55kDa
125kDa
102kDa
43kDa
35kDa
Q
Relative PGK1 protein level
R
Relative LDHA protein level
S
T
Relative GLUT1 protein level
U
Relative HK1 protein level
V
Relative HK2 protein level
W
Relative PGK1 protein level
X
Relative LDHA protein level

Figure 5. SETD2 overexpression inhibited TKT expression and suppressed glycolysis. (A, B) WB analysis of TKT level in A549 and H1299 cells after transfection with OE-TKT or si-TKT. (C-H) TKT overexpression reversed OE-SETD2-induced suppression of glucose uptake (C, D), lactate production (E, F), and ATP content (G, H). (I-L) TKT overexpression reversed OE-SETD2-induced reduction in ECAR. (M-X) WB analysis of glycolysis-related proteins GLUT1, HK1, HK2, PGK1 and LDHA after co-transfection with OE-TKT and OE-SETD2. Note: ECAR, Extracellular acidification rate. $^{**}P<0.01$, $^{***}P<0.001$ vs OE-NC/si-NC; ns $P\geq0.05$ vs OE-SETD2/si-SETD2; $^{\#}P<0.05$, $^{\#\#}P<0.01$, $^{\#\#\#}P<0.001$ vs OE-SETD2+OE-NC/si-SETD2+si-NC.

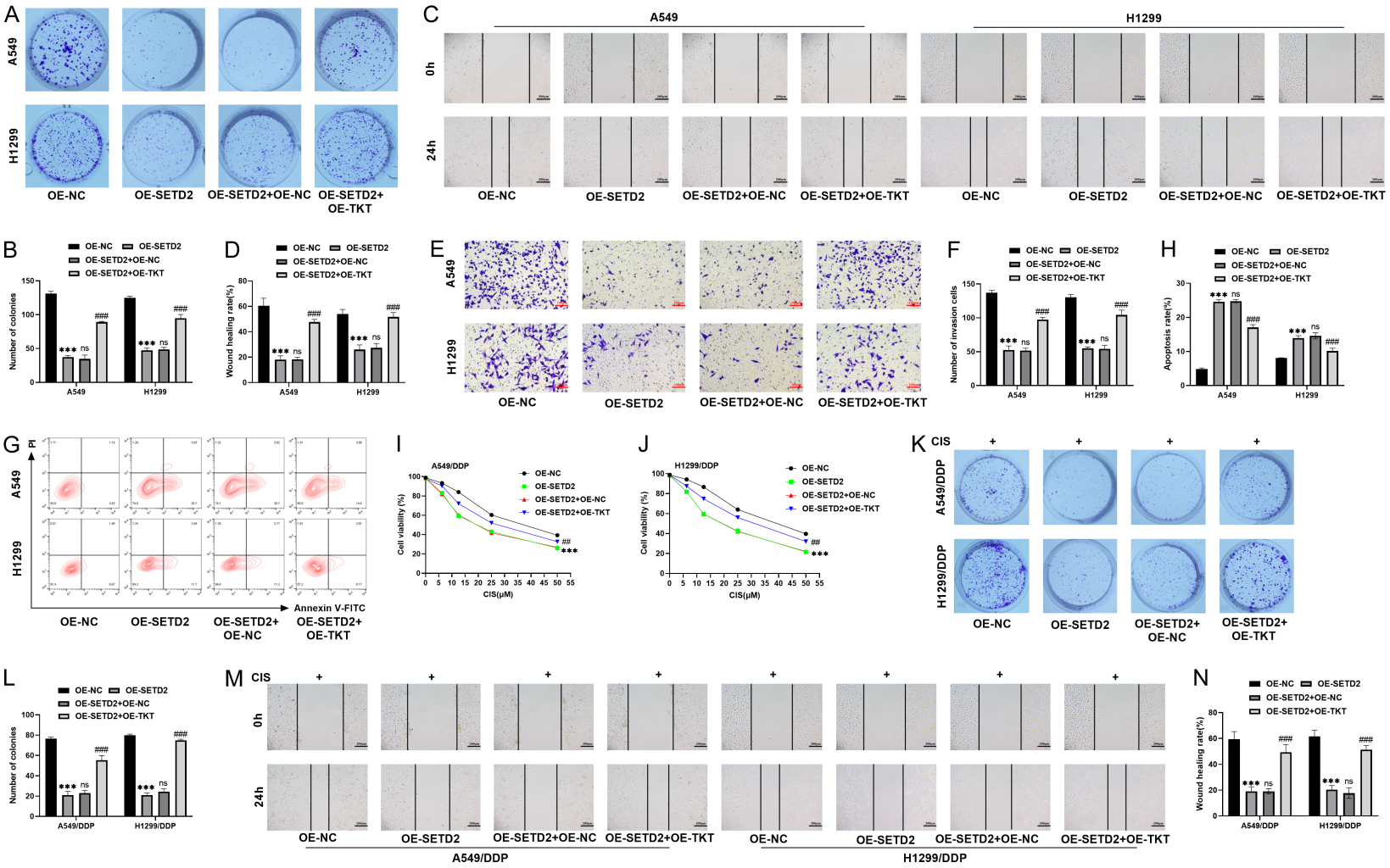

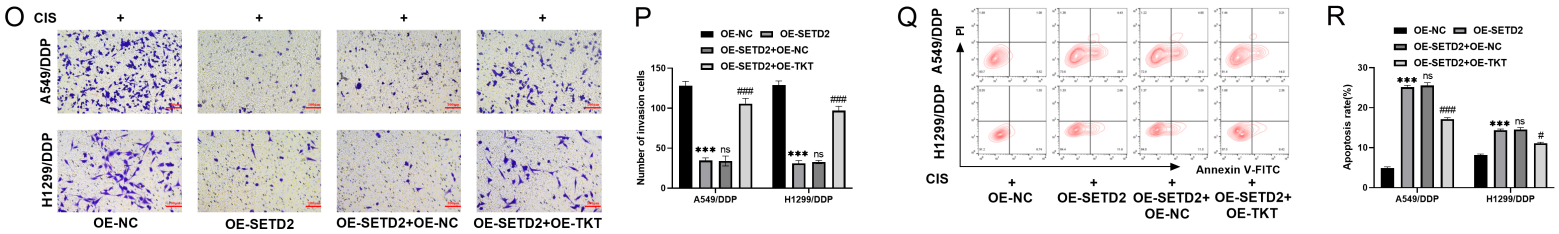

Figure 6. SETD2 overexpression suppressed malignant progression of LUAD and enhanced chemosensitivity through regulation of TKT. (A-H) Effects of co-transfection with OE-SETD2 and OE-TKT on colony formation (A, B), scratch healing rate (10×, 200 μm) (C, D), number of invaded cells (20×, 100 μm) (E, F), and apoptosis rate (G, H) in H1299 and A549 cells. (I, J) Effects of co-transfection with OE-SETD2 and OE-TKT on cell viability after CIS treatment assessed by CCK-8 assay. (K-R) Effects of co-transfection with OE-SETD2 and OE-TKT on colony formation (K, L), scratch healing rate (10×, 200 μm) (M, N), number of invaded cells (20×, 100 μm) (O, P), and apoptosis rate (Q, R) in H1299/DDP and A549/DDP cells after CIS treatment. ***P<0.001 vs OE-NC; ns P≥0.05 vs OE-SETD2; $^{\#}P$<0.05, $^{\#\#}P$<0.01, $^{\#\#\#}P$<0.001 vs OE-SETD2+OE-NC.

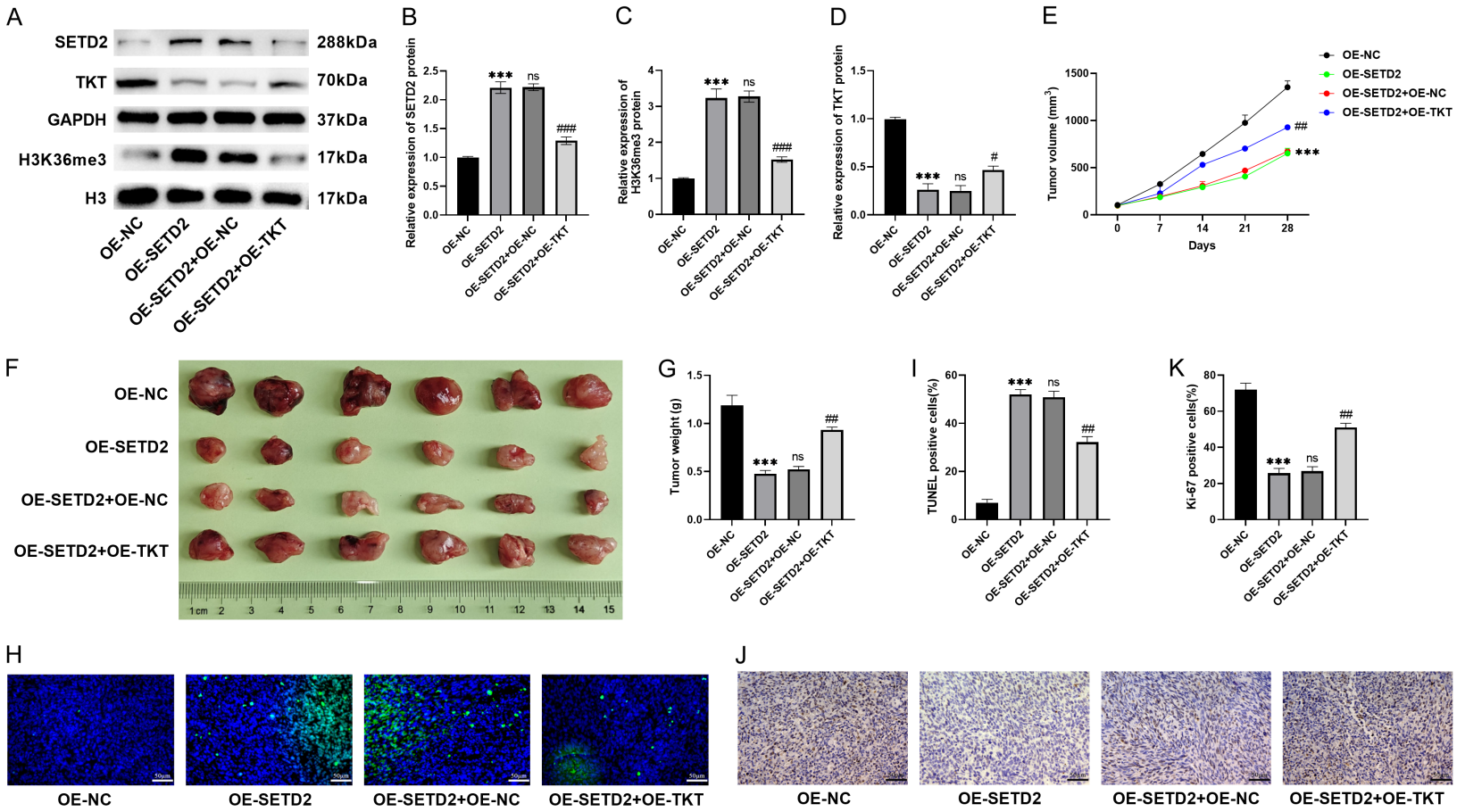

Figure 7. SETD2 overexpression suppressed A549 cell-transplanted tumor growth *in vivo* via regulating TKT. A-D. WB analysis of SETD2, H3K36me3, and TKT levels in xenograft tumor tissues. E-G. Xenograft tumor volume and weight. H, I. TUNEL-positive cells in xenograft tumor tissues (40×, 50 μm). J, K. Immunohistochemical staining of Ki-67 in xenograft tumor tissues (40×, 50 μm). ***P<0.001 vs OE-NC; ns P≥0.05 vs OE-SETD2; $^{\#}P$<0.05, $^{\#\#}P$<0.01, $^{\#\#\#}P$<0.001 vs OE-SETD2+OE-NC.

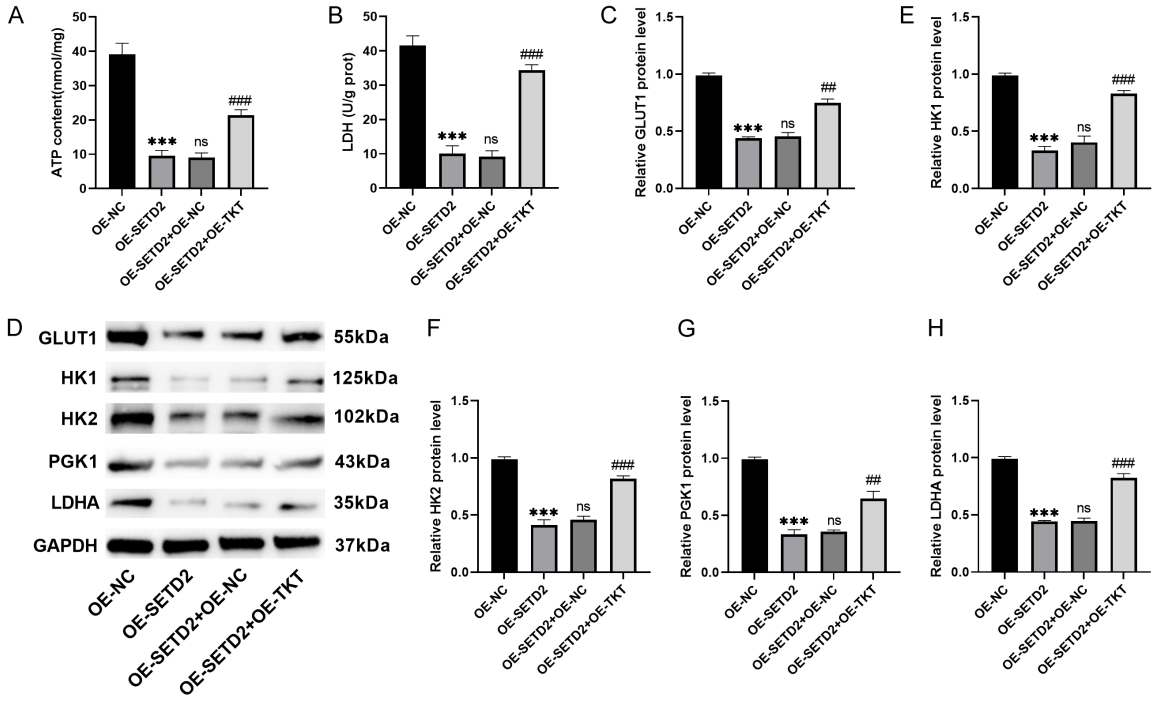

Figure 8. SETD2 overexpression reduced glycolysis in vivo by inhibiting TKT. (A, B) ATP concentration (A) and LDH activity (B) in xenograft tumor tissues. (C-H) WB analysis of glycolysis-related proteins GLUT1, HK1, HK2, PGK1 and LDHA after co-transfection with OE-SETD2 and OE-TKT. Note: LDH, lactate dehydrogenase. ***P<0.001 vs OE-NC; ns P≥0.05 vs OE-SETD2; ##P<0.01, ###P<0.001 vs OE-SETD2+OE-NC.

These *in vivo* results demonstrate that SETD2 overexpression inhibits LUAD xenograft growth through down-regulation of TKT expression, while overexpression of TKT counteracts the tumor-suppressive effect of SETD2.

SETD2 overexpression reduced glycolysis in vivo by inhibiting TKT

Whether SETD2 regulates glycolysis in LUAD *in vivo* via modulation of TKT was further examined. ATP levels (**Figure 8A**) and LDH activity (**Figure 8B**) were markedly reduced in tumor tissues of the OE-SETD2 group, suggesting that SETD2 overexpression inhibited the glycolytic metabolism in tumors. In contrast, after co-transfection with OE-TKT, both ATP concentration and LDH activity in tumor tissues were significantly increased, indicating that overexpression of TKT effectively reduced the inhibitory effect of SETD2 on glycolytic metabolism. In addition, protein levels of key glycolytic regulators, including GLUT1, HK1, HK2, PGK1, and LDHA, was significantly reduced in the OE-SETD2 group. Co-transfection with OE-TKT significantly restored the levels of these proteins (**Figure 8C-H**). These results suggest that SETD2 overexpression inhibits glycolytic metabolism in tumor tissues *in vivo* by suppressing TKT expression.

SETD2 overexpression enhanced tumor sensitivity to CIS in vivo

Finally, to explore whether SETD2 modulates chemosensitivity *in vivo,* a nude mouse xenograft model was established using subcutaneous transplantation of A549/DDP cells and further challenged with CIS. Overexpression of SETD2 significantly reduced tumor volume and weight, whereas co-transfection with OE-TKT (OE-SETD2+OE-TKT) significantly reversed these tumor growth-inhibitory effects (**Figure 9A-C**). Western blot analysis showed that SETD2 and H3K36me3 protein levels were significantly increased, while the TKT level was significantly decreased in the OE-SETD2 group. Co-transfection with OE-TKT reduced SETD2 and H3K36me3 expression, while increasing TKT levels (**Figure 9D**, **9E**). In addition, the expression levels of resistance-associated proteins, including MRP1, ABCB1, and ABCG2 were significantly reduced in the OE-SETD2 group; and TKT overexpression reversed the

down-regulation trend of these resistance-associated proteins (**Figure 9F**, **9G**). Furthermore, the proportion of TUNEL-positive cells was significantly increased and the Ki-67 level was significantly decreased in the OE-SETD2 group, which were partially reversed after co-transfection with OE-TKT (**Figure 9H-K**). These results confirm that SETD2 overexpression enhances the chemosensitivity of LUAD xenograft tumors, whereas overexpression of TKT diminishes the chemosensitizing effects of SETD2, further clarifying the important role of the SETD2-TKT axis in LUAD chemoresistance.

Discussion

LUAD is a major histological subtype of lung cancer, characterized by high morbidity and mortality worldwide [33]. Identifying specific targets for LUAD treatment is critical for improving the prognosis and survival of patients. Epigenetic dysregulations are key driving factors for LUAD initiation and development. Histone methyltransferase play central roles in epigenetic regulation, and their dysfunction has been closely related to tumor prognosis [34-36]. A previous study has shown that SETD2 levels are decreased in human LUAD tissues and cells, and SETD2 overexpression can inhibit the growth and migration of LUAD cells [36]. Based on GEPIA2 database analysis and WB verification, this study discovered that SETD2 was markedly reduced in both LUAD tissues and cell lines, although no statistical correlation was observed between its expression level and patients' overall survival. However, it has been shown that SETD2 is downregulated in tumors such as gastric cancer [37] and prostate cancer [38], and patients with low SETD2 expression have a poorer prognosis. In addition, SETD2 overexpression inhibited the malignant biological properties of LUAD cells (H1299 and A549) and promoted apoptosis, while SETD2 knockdown resulted in opposite outcomes, confirming that SETD2 functions as a tumor suppressor gene in LUAD. This result is consistent with the classical mechanism of SETD2 regulating gene transcription by catalyzing H3K36me3 modification. H3K36me3 is a critical epigenetic mark involved in transcriptional regulation, genomic stability, and DNA damage repair. Loss of H3K36me3 has been shown to result in transcriptional silencing of tumor suppressor genes and abnormal activation of oncogenes, thus promoting malignant tumor progression [12, 39, 40]. Notably, SETD2 expression was significantly lower in CIS-resistant cell lines (H1299/DDP and A549/DDP) than in parental cells, implying that SETD2 loss may contribute to the development of chemotherapy resistance in LUAD, which provides a new entry point for addressing the bottleneck of clinical LUAD chemotherapy.

Tumor metabolic reprogramming, especially the Warburg effect, is a hallmark that distinguishes tumor cells from normal cells. Tumor cells produce energy and biosynthetic precursors through glycolysis even under oxygen-sufficient conditions [41, 42]. Glycolysis not only supplies energy to support rapid tumor cell proliferation and migration, but also participates in critical pathological processes, including chemotherapy resistance, DNA repair, and immune escape [43, 44]. Research has confirmed a significant link between the aberrant activation of the glycolytic pathway and the onset, advancement, and chemotherapy resistance in LUAD [45, 46]. Therefore, targeting tumor glycolytic represents a promising strategy for LUAD treatment.

In our study, overexpression of SETD2 decreased glucose uptake, lactate production, ATP content, and ECAR level in LUAD cells, directly indicating suppression of glycolytic activity. At the molecular level, SETD2 overexpression downregulated the expression of key glycolysis-related proteins, including GLUT1, HK1, HK2, PGK1 and LDHA, while SETD2 knockdown reversed these effects. Zhu *et al*. reported that SETD2 knockdown increased glycolytic activity in an osteomyelitis cell model, suggesting that SETD2 may inhibit glycolysis in different disease models [47]. Previous studies have indicated that drug-resistant cells often rely on enhanced glycolysis to withstand the cytotoxic stress imposed by chemotherapeutic drugs [48, 49]. In line with these findings, in this study, SETD2 was markedly reduced in CIS-resistant cells, and its overexpression reversed the drug resistance phenotype, suggesting that SETD2 may improve the chemosensitivity of CIS-resistant cells by inhibiting glycolysis and breaking the metabolic adaptability required for drug resistance.

To further elucidate the molecular mechanism by which SETD2 inhibits glycolysis and enhanc-

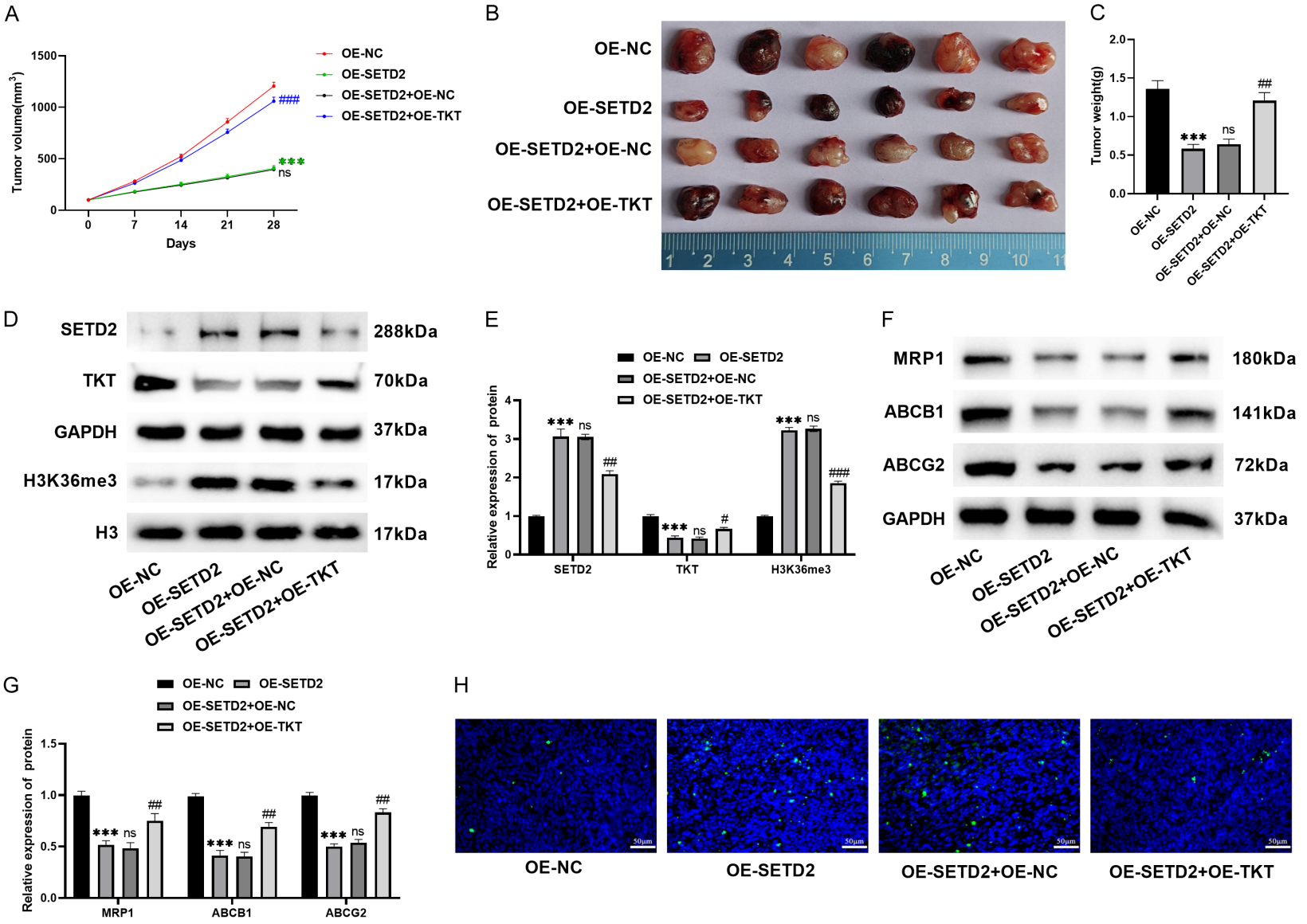
A
Tumor volume(mm3)
Days
OE-NC
OE-SETD2
OE-SETD2+OE-NC
OE-SETD2+OE-TKT
B
C
Tumor weight(g)
D
SETD2
TKT
GAPDH
H3K36me3
H3
288kDa
70kDa
37kDa
17kDa
17kDa
E
Relative expression of protein
F
MRP1
ABCB1
ABCG2
GAPDH
180kDa
141kDa
72kDa
37kDa
G
Relative expression of protein
H
50μm

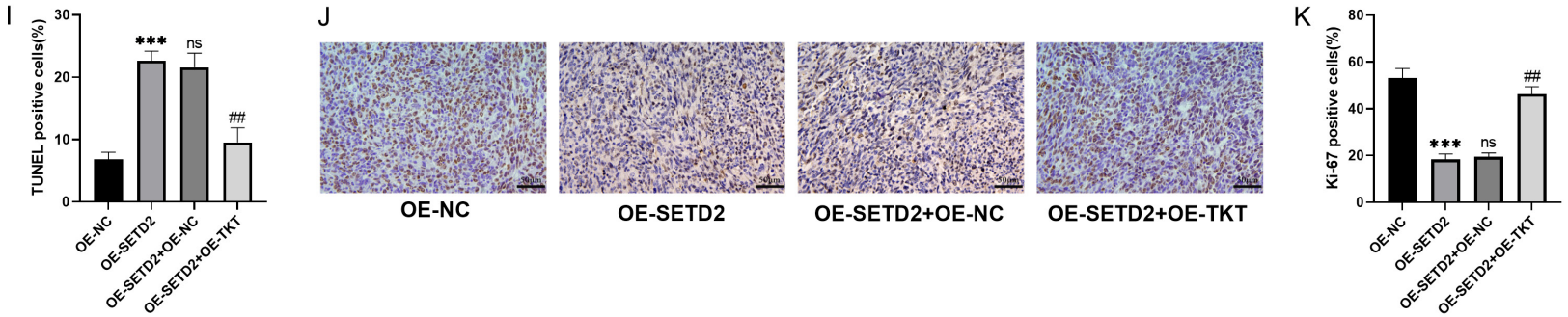

Figure 9. SETD2 overexpression enhanced chemosensitivity *in vivo*. A-C. Xenograft tumor volume and weight (A549/DDP cell transplanted tumor). D, E. WB analysis of SETD2, H3K36me3 and TKT protein expression in tumor tissues. F, G. WB analysis of drug resistance-associated proteins MRP1, ABCB1, and ABCG2 in tumor tissues. H, I. TUNEL staining and quantitative analysis of apoptotic cells in tumor tissues (40×, 50 μm). J, K. Immunohistochemical analysis of Ki-67 expression in tumor tissues (40×, 50 μm). $^{***}P<0.001$ vs OE-NC; ns $P\geq0.05$ vs OE-SETD2; $^{\#\#}P<0.01$ vs OE-SETD2+OE-NC.

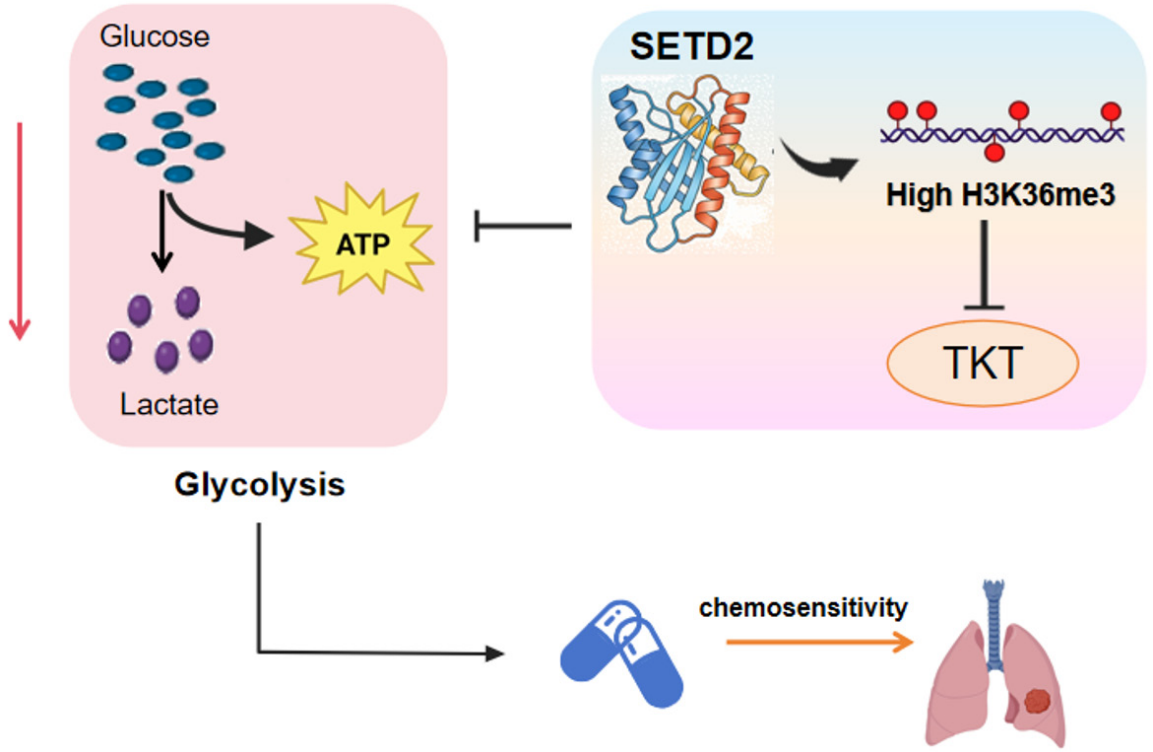

Figure 10. Schematic diagram illustrating the mechanism underlying SETD2-mediated regulation of LUAD chemosensitivity.

es chemosensitivity, we investigated the downstream target genes of SETD2. TKT, a crucial enzyme in the PPP, is highly expressed in various tumors and essential for the maintenance of cell growth [22, 50]. Our previous research found that elevated TKT expression was linked to advanced tumor stage in LUAD, and TKT inhibitors induced LUAD cell cycle arrest and apoptosis [23]. In CIS-resistant non-small cell lung cancer cells, suppressing TKT expression inhibits cell proliferation and reverses the drug-resistant phenotype [51]. Importantly, SETD2 also regulates the transcriptional level of TKT in pancreatic cancer cells [18]. In this study, TKT displayed diminished expression in HEK293T cells but markedly elevated expression in LUAD cells, displaying an inverse expression pattern relative to SETD2. SETD2 overexpression significantly reduced TKT protein expression, whereas SETD2 knockdown upregulated TKT expression, indicating that SETD2 negatively regulates TKT. Moreover, TKT overexpression partially reversed the suppressive impact of SETD2 on the malignant phenotype and glycolysis in LUAD cells and attenuated the SETD2-mediated enhancement of chemosensitivity of CIS-resistant cells. Consistently, *in vivo* experiments further confirmed that TKT overexpression attenuated the tumor-suppressive effect mediated by SETD2 overexpression.

Taken together, SETD2 suppresses glycolytic metabolism by downregulating TKT expression, which in turn inhibits LUAD malignant progression and reverses chemoresistance (**Figure 10**). This study extends the regulatory relationship between the histone methyltransferase SETD2 and TKT - a core enzyme of the non-oxidative PPP - to the context of LUAD, providing a new insights into the cross-regulatory network of epigenetic modification and metabolic reprogramming in LUAD.

This study still has several limitations. First, the prognostic value of SETD2 in LUAD was evaluated based on a single public database cohort. Multicenter clinical samples were not included for validation, and multivariate analysis adjusting for confounding factors, such as tumor stage and differentiation degree, were not performed. Therefore, it remains inconclusive whether SETD2 serves as an independent prognostic biomarker in LUAD. Second, although this study identified the SETD2-TKT axis

as a critical regulator of glycolytic metabolism, the underlying metabolic mechanisms have not been fully elucidated. Specifically, quantitative detection of PPP intermediates and metabolic flux tracing analyses were not performed, making it difficult to accurately characterize the specific mechanism by which this regulatory axis affects cellular metabolic pathways. To address these limitations, future research should expand clinical sample size and conduct multi-center validation to clarify the independent prognostic value of SETD2. Simultaneously, by combining PPP intermediate quantification and metabolic flux tracing technologies, the metabolic regulation mechanism mediated by the SETD2-TKT axis should be further refined to provide a more robust theoretical basis for the translational application of this pathway.

Conclusion

SETD2 is downregulated in LUAD, and its loss contributes to enhanced glycolytic activity by relieving transcriptional repression of the TKT gene, thereby promoting tumor progression and chemoresistance. By directly binding to the TKT locus and modulating its transcriptional activity, SETD2 suppresses glycolytic metabolism, inhibits LUAD progression, and enhances the chemosensitivity of CIS-resistant cells. I*n vivo* experiments likewise confirmed the tumor suppressive impact of the SETD2/TKT axis. This study preliminarily elucidates the underlying mechanism by which SETD2 inhibits the malignant progression of LUAD, highlighting the SETD2-TKT axis as a potential molecular target for therapeutic intervention for LUAD.

Acknowledgements

This work was supported by the key project from the Huadong Hospital, Fudan University (No. GZRPY003Y).

Disclosure of conflict of interest

None.

Abbreviations

LUAD, Lung adenocarcinoma; SETD2, SET domain-containing protein 2; CCK-8, Cell Counting Kit-8; TKT, Transketolase; CIS, Cis-platinum; H3K36me3, Histone H3 lysine 36 trimethylation; PI, Prodium Iodide; ECAR, Extracellular acidification rate; ChIP, Chromatin immunoprecipitation; BSA, Bovine serum albumin; LDH, Lactic dehydrogenase; ATP, Adenosine Triphosphate; WB, Western blot; GLUT1, GGlucose transporter 1; HK1, Hexokinase 1; HK2, Hexokinase 2; PGK1, Phosphoglycerate kinase 1; LDHA, Lactate Dehydrogenase A; MRP1, multidrug resistance-associated protein 1; ABCB1, ATP-binding cassette sub-family B member 1; ABCG2, ATP binding cassette subfamily G member 2; H3, Histone H3; PPP, pentose phosphate pathway.

Address correspondence to: Hui Zhao, Department of Respiratory and Critical Care Medicine, The Second Affiliated Hospital of Anhui Medical University, No. 678 Furong Road, Hefei 230601, Anhui, China. E-mail: zhaohuichenxi@126.com

References

[1] Siegel RL, Kratzer TB, Giaquinto AN, Sung H and Jemal A. Cancer statistics, 2025. CA Cancer J Clin 2025; 75: 10-45.

[2] Wu Y, He S, Cao M, Teng Y, Li Q, Tan N, Wang J, Zuo T, Li T, Zheng Y, Xia C and Chen W. Comparative analysis of cancer statistics in China and the United States in 2024. Chin Med J (Engl) 2024; 137: 3093-3100.

[3] Wei X, Li X, Hu S, Cheng J and Cai R. Regulation of ferroptosis in lung adenocarcinoma. Int J Mol Sci 2023; 24: 14614.

[4] Song Y, Kelava L and Kiss I. MiRNAs in lung adenocarcinoma: role, diagnosis, prognosis, and therapy. Int J Mol Sci 2023; 24: 13302.

[5] Sengupta D, Zeng L, Li Y, Hausmann S, Ghosh D, Yuan G, Nguyen TN, Lyu R, Caporicci M, Morales Benitez A, Coles GL, Kharchenko V, Czaban I, Azhibek D, Fischle W, Jaremko M, Wistuba, II, Sage J, Jaremko Ł, Li W, Mazur PK and Gozani O. NSD2 dimethylation at H3K36 promotes lung adenocarcinoma pathogenesis. Mol Cell 2021; 81: 4481-92.e9.

[6] Li Z, Chen S, He X, Gong S, Sun L and Weng L. SLC3A2 promotes tumor-associated macrophage polarization through metabolic reprogramming in lung cancer. Cancer Sci 2023; 114: 2306-17.

[7] Wu J, Chen Y, Zou H, Xu K, Hou J, Wang M, Tian S, Gao M, Ren Q, Sun C, Lu S, Wang Q, Shu Y, Wang S and Wang X. 6-Phosphogluconate dehydrogenase promotes glycolysis and fatty acid synthesis by inhibiting the AMPK pathway in lung adenocarcinoma cells. Cancer Lett 2024; 601: 217177.

[8] Feng B, Wang X, Qiu D, Sun H, Deng J, Tan Y, Ji K, Xu S, Zhang S and Tang C. DDX18 facilitates the tumorigenesis of lung adenocarcinoma by

promoting cell cycle progression through the upregulation of CDK4. Int J Mol Sci 2024; 25: 4953.
[9] Li X, Wang Y, Liu Y and Meng Q. Opsin3 regulates cell proliferation, migration, and apoptosis in lung adenocarcinoma via GPX3 pathway. Eur J Med Res 2025; 30: 343.
[10] Zhao G, Liang J, Shan G, Gu J, Xu F, Lu C, Ma T, Bi G, Zhan C and Ge D. KLF11 regulates lung adenocarcinoma ferroptosis and chemosensitivity by suppressing GPX4. Commun Biol 2023; 6: 570.
[11] Huang Y, Wu G, Bi G, Cheng L, Liang J, Li M, Zhang H, Shan G, Hu Z, Chen Z, Lin Z, Jiang W, Wang Q, Xi J, Yin S and Zhan C. Unveiling chemotherapy-induced immune landscape remodeling and metabolic reprogramming in lung adenocarcinoma by scRNA-sequencing. Elife 2024; 13: RP95988.
[12] He J, Xu T, Zhao F, Guo J and Hu Q. SETD2-H3K36ME3: an important bridge between the environment and tumors. Front Genet 2023; 14: 1204463.
[13] Mason FM, Kounlavong ES, Tebeje AT, Dahiya R, Guess T, Khan A, Vlach L, Norris SR, Lovejoy CA, Dere R, Strahl BD, Ohi R, Ly P, Walker CL and Rathmell WK. SETD2 safeguards the genome against isochromosome formation. Proc Natl Acad Sci U S A 2023; 120: e2303752120.
[14] Sharda A and Humphrey TC. The role of histone H3K36me3 writers, readers and erasers in maintaining genome stability. DNA Repair (Amst) 2022; 119: 103407.
[15] Rao H, Liu C, Wang A, Ma C, Xu Y, Ye T, Su W, Zhou P, Gao WQ, Li L and Ding X. SETD2 deficiency accelerates sphingomyelin accumulation and promotes the development of renal cancer. Nat Commun 2023; 14: 7572.
[16] Ma C, Liu M, Feng W, Rao H, Zhang W, Liu C, Xu Y, Wang Z, Teng Y, Yang X, Ni L, Xu J, Gao WQ, Lu B and Li L. Loss of SETD2 aggravates colorectal cancer progression caused by SMAD4 deletion through the RAS/ERK signalling pathway. Clin Transl Med 2023; 13: e1475.
[17] Niu N, Shen X, Zhang L, Chen Y, Lu P, Yang W, Liu M, Shi J, Xu D, Tang Y, Yang X, Weng Y, Zhao X, Wu LM, Sun Y and Xue J. Tumor cell-intrinsic SETD2 deficiency reprograms neutrophils to foster immune escape in pancreatic tumorigenesis. Advanced science (Weinheim, Baden-Wurttemberg, Germany) 2023; 10: e2202937.
[18] Shen X, Chen Y, Liu M, Shi J, Tang Y, Yang X, Xu D, Yao H, Lu P, Sun Y, Xue J and Niu N. Glycolysis addiction compensating for a defective pentose phosphate pathway confers gemcitabine sensitivity in SETD2-deficient pancreatic cancer. Biochem Biophys Res Commun 2022; 615: 9-16.
[19] Walter DM, Gladstein AC, Doerig KR, Natesan R, Baskaran SG, Gudiel AA, Adler KM, Acosta JO, Wallace DC, Asangani IA and Feldser DM. Setd2 inactivation sensitizes lung adenocarcinoma to inhibitors of oxidative respiration and mTORC1 signaling. Commun Biol 2023; 6: 255.
[20] Hao S, Meng Q, Sun H, Li Y, Li Y, Gu L, Liu B, Zhang Y, Zhou H, Xu Z and Wang Y. The role of Transketolase in human cancer progression and therapy. Biomed Pharmacother 2022; 154: 113607.
[21] Zhen X, Zhang M, Hao S and Sun J. Glucose-6-phosphate dehydrogenase and Transketolase: key factors in breast cancer progression and therapy. Biomed Pharmacother 2024; 176: 116935.
[22] Li M, Zhao X, Yong H, Xu J, Qu P, Qiao S, Hou P, Li Z, Chu S, Zheng J and Bai J. Transketolase promotes colorectal cancer metastasis through regulating AKT phosphorylation. Cell Death Dis 2022; 13: 99.
[23] Niu C, Qiu W, Li X, Li H, Zhou J and Zhu H. Transketolase serves as a biomarker for poor prognosis in human lung adenocarcinoma. J Cancer 2022; 13: 2584-93.
[24] Zhang L, Huang Z, Cai Q, Zhao C, Xiao Y, Quan X, Tang C and Gao J. Inhibition of Transketolase improves the prognosis of colorectal cancer. Front Med (Lausanne) 2022; 9: 837143.
[25] Fu M, Zhang M, Zhang L, Feng Y, Gao C, Xu H, Zhang J, Zhang H, Peng T, Chu Y, Wu Y, Wang P, Ye D, Mao Y and Hua W. Transketolase attenuates the chemotherapy sensitivity of glioma cells by modulating R-loop formation. Cell Rep 2025; 44: 115142.
[26] Xie H, Yao J, Wang Y and Ni B. Exosome-transmitted circVMP1 facilitates the progression and cisplatin resistance of non-small cell lung cancer by targeting miR-524-5p-METTL3/SOX2 axis. Drug Deliv 2022; 29: 1257-71.
[27] Beeraka NM, Nagalakshmi A, Satyavathi A, Kote DM, Reddy Y P, Basappa B, Nikolenko VN, Bannimath G, Bulygin KV and P A M. Ginsenoside Rh4 suppresses Notch3 and PI3K/Akt pathway to inhibit growth and metastasis of gastric cancer cells. Journal of Cancer Biomoleculars and Therapeutics 2025; 2: 145-56.
[28] Li XQ, Cao ZR, Deng M, Qing Y, Sun L and Wu ZJ. E2F8-TPX2 axis regulates glycolysis and angiogenesis to promote progression and reduce chemosensitivity of liver cancer. Cytotechnology 2024; 76: 817-32.
[29] Zeng C, Huang D, Wang L, Liang H and Ma X. Silencing ZIC5 suppresses glycolysis and promotes disulfidptosis in lung adenocarcinoma cells. Cancer Biol Ther 2025; 26: 2501780.
[30] Wang X, Wang Z, Huang R, Lu Z, Chen X and Huang D. UPP1 promotes lung adenocarcino-

ma progression through epigenetic regulation of glycolysis. Aging Dis 2022; 13: 1488-503.
[31] Zhao R, Zhao D, Zhu X, Li F, Xiong P, Li S and Liu J. The Influence of miR-3149 on the malignancy progression of gastric cancer by negatively regulating CEACAM5. Journal of Cancer Biomoleculars and Therapeutics 2024; 1: 1-10.
[32] Wang L, Wang D, Xu Z, Qiu Y, Chen G and Tan F. Circ_0010235 confers cisplatin resistance in lung cancer by upregulating E2F7 through absorbing miR-379-5p. Thorac Cancer 2023; 14: 1946-57.
[33] Smolarz B, Łukasiewicz H, Samulak D, Piekarska E, Kołaciński R and Romanowicz H. Lung cancer-epidemiology, pathogenesis, treatment and molecular aspect (Review of Literature). Int J Mol Sci 2025; 26: 2049.
[34] Bajbouj K, Al-Ali A, Ramakrishnan RK, Saber-Ayad M and Hamid Q. Histone modification in NSCLC: molecular mechanisms and therapeutic targets. Int J Mol Sci 2021; 22: 11701.
[35] Lazaro-Camp VJ, Salari K, Meng X and Yang S. SETDB1 in cancer: overexpression and its therapeutic implications. Am J Cancer Res 2021; 11: 1803-27.
[36] Yang X, Chen R, Chen Y, Zhou Y, Wu C, Li Q, Wu J, Hu WW, Zhao WQ, Wei W, Shi JT and Ji M. Methyltransferase SETD2 inhibits tumor growth and metastasis via STAT1-IL-8 signaling-mediated epithelial-mesenchymal transition in lung adenocarcinoma. Cancer Sci 2022; 113: 1195-207.
[37] Feng W, Ma C, Rao H, Zhang W, Liu C, Xu Y, Aji R, Wang Z, Xu J, Gao WQ and Li L. Setd2 deficiency promotes gastric tumorigenesis through inhibiting the SIRT1/FOXO pathway. Cancer Lett 2023; 579: 216470.
[38] Gamallat Y, Felipe Lima J, Seyedi S, Li Q, Rokne JG, Alhajj R, Ghosh S and Bismar TA. Exploring the prognostic significance of SET-domain containing 2 (SETD2) expression in advanced and castrate-resistant prostate cancer. Cancers (Basel) 2024; 16: 1436.
[39] Michail C, Rodrigues Lima F, Viguier M and Deshayes F. Structure and function of the lysine methyltransferase SETD2 in cancer: from histones to cytoskeleton. Neoplasia 2025; 59: 101090.
[40] Zhou X, Sekino Y, Li HT, Fu G, Yang Z, Zhao S, Gujar H, Zu X, Weisenberger DJ, Gill IS, Tulpule V, D'Souza A, Quinn DI, Han B and Liang G. SETD2 Deficiency confers sensitivity to dual inhibition of DNA methylation and PARP in kidney cancer. Cancer Res 2023; 83: 3813-26.
[41] Barba I, Carrillo-Bosch L and Seoane J. Targeting the Warburg effect in cancer: where do we stand? Int J Mol Sci 2024; 25: 3142.
[42] Bose S, Zhang C and Le A. Glucose metabolism in cancer: the Warburg effect and beyond. Adv Exp Med Biol 2021; 1311: 3-15.
[43] Chen H, Li Y, Li H, Chen X, Fu H, Mao D, Chen W, Lan L, Wang C, Hu K, Li J, Zhu C, Evans I, Cheung E, Lu D, He Y, Behrens A, Yin D and Zhang C. NBS1 lactylation is required for efficient DNA repair and chemotherapy resistance. Nature 2024; 631: 663-9.
[44] Guo D, Tong Y, Jiang X, Meng Y, Jiang H, Du L, Wu Q, Li S, Luo S, Li M, Xiao L, He H, He X, Yu Q, Fang J and Lu Z. Aerobic glycolysis promotes tumor immune evasion by hexokinase2-mediated phosphorylation of IκBα. Cell Metab 2022; 34: 1312-24, e6.
[45] Wang M, He T, Meng D, Lv W, Ye J, Cheng L and Hu J. BZW2 modulates lung adenocarcinoma progression through glycolysis-mediated IDH3G lactylation modification. J Proteome Res 2023; 22: 3854-65.
[46] Liu G, Liu X, Zeng W and Zhou W. TFAP2A upregulates SKA3 to promote glycolysis and reduce the sensitivity of lung adenocarcinoma cells to cisplatin. Pharmacology 2024; 109: 202-215.
[47] Zhu D, Chen F, Qiang H and Qi H. SPA inhibits hBMSC osteogenic differentiation and M1 macrophage polarization by suppressing SETD2 in acute suppurative osteomyelitis. Sci Rep 2024; 14: 12728.
[48] Wang Y, Yuan J, Liu J, Li X, Zhou C, Qian M, Zou Z, Lu C, Huang G and Jin M. Melittin suppresses aerobic glycolysis by regulating HSF1/PDK3 to increase chemosensitivity of NSCLC. Eur J Pharmacol 2025; 986: 177084.
[49] Song CW, Kim H, Kim MS, Park HJ, Paek SH, Terezakis S and Cho LC. Role of HIF-1α in the responses of tumors to radiotherapy and chemotherapy. Cancer Res Treat 2025; 57: 1-10.
[50] Hao S, Meng Q, Sun H, Yang X, Liu B, Zhang Y, Zhou H, Xu Z and Wang Y. Human papillomavirus type 16 E6 promotes cervical cancer proliferation by upregulating Transketolase enzymatic activity through the activation of protein kinase B. Mol Carcinog 2024; 63: 339-355.
[51] Li S, Lu Z, Jiang W, Xu Y, Chen R, Wang J, Jiao B and Lu X. Chaetocin, a natural inhibitor of Transketolase, suppresses the non-oxidative pentose phosphate pathway and inhibits the growth of drug-resistant non-small cell lung cancer. Antioxidants (Basel) 2025; 14: 330.